

Luminosity and stellar mass functions of disks and spheroids in the SDSS and the supermassive black hole mass function

A. J. Benson¹, Dajana Džanović², C. S. Frenk², Ray Sharples²

1. Theoretical Astrophysics, Caltech, MC130-33, 1200 E. California Blvd., Pasadena, CA 91125, U.S.A. (e-mail: abenson@its.caltech.edu)

2. Institute for Computational Cosmology, University of Durham, Science Laboratories, South Road, Durham, DH1 3LE, U.K.

15 October 2018

ABSTRACT

Using the GALACTICA code of Benson et al., we obtain quantitative measurements of spheroid-to-disk ratios for a sample of 8839 galaxies observed in the Sloan Digital Sky Survey. We carry out extensive tests of this code and of GIM2D, finding that they perform similarly in all respects. From the spheroid and disk luminosities, we construct luminosity and stellar mass functions for each component and estimate the relative luminosity and stellar mass densities of disks and spheroids in the local Universe. Assuming a simple one-to-one mapping between spheroid mass and the mass of a central supermassive black hole, we provide the most accurate determination so far of the black hole mass function in the local universe. From this, we infer a cosmological mass density of black holes of $\rho_{\bullet} = (3.77 \pm 0.97) \times 10^5 h M_{\odot} \text{Mpc}^{-3}$. We compare our results to predictions from current hierarchical models of galaxy formation and these are found to fare well in predicting the qualitative trends observed. We find that stars in disks contribute 35–51% of the local stellar mass density.

Key words: galaxies: structure; galaxies: abundances; galaxies: bulges; galaxies: luminosity function, mass function; galaxies: statistics

1 INTRODUCTION

The distinction between disks and spheroids is one of the defining properties of galaxies. Determining the relative importance of these two basic types of galactic component is fundamental to a broad characterization of the galaxy population. Yet, this is a complicated task which requires not only high quality imaging for large samples, but also software capable of decomposing the light from each object into a disk and a spheroid¹. The determination of spheroid luminosities has recently received even more prominence since the discovery that perhaps all galaxies harbour a supermassive black hole at their centre whose mass is proportional to the luminosity of the spheroid or bulge (Kormendy & Richstone 1995; Magorrian et al. 1998; Merritt & Ferrarese 2001; Marconi & Hunt 2003; Häring & Rix 2004).

From a theoretical point of view, explaining why most of the stars in the Universe end up either in disks or in spheroids and understanding the physical processes that result in the formation of one or the other of these morpholog-

ical structures is a major challenge. The current theoretical framework used to investigate galaxy formation is the cold dark matter model (Peebles 1982, Blumenthal et al. 1984, Davis et al. 1985), in which galaxies build up hierarchically. Within this model, the basic processes thought to be responsible for the distinction between disks and spheroids were identified over twenty years ago (Fall 1979, Frenk et al. 1985): disks result from the collapse of rotating gas cooling within dark matter halos whereas spheroids result from major mergers or disk instabilities (Fall & Efstathiou 1980; Barnes & Hernquist 1992; Mo, Mao & White 1998). The traditional categories of galaxy morphology, spirals, irregulars, etc, are too detailed for current theoretical models to explain, but the relative luminosities and stellar masses of spheroids and disks can readily be predicted (Kauffmann, White & Guiderdoni 1993; Baugh et al. 1996a; Baugh et al. 1996b; Kauffmann, Charlot & White 1996; Kauffmann & Charlot 1998; Somerville & Primack 1999; Hatton et al. 2003). Thus, accurate measurements of these quantities, for example, as a function of absolute magnitude and in different environments provides a powerful test of models of galaxy formation and evolution.

¹ We will use the term “spheroid” throughout to refer to both elliptical galaxies and the bulges of spiral galaxies.

tions of spheroids and disks to the luminosity density of the Universe was made by Schechter & Dressler (1987). They studied a magnitude limited sample of ~ 200 galaxies brighter than $V = 16.5$, drawn from the catalogue of Dressler (1980a), and determined spheroid-to-disk ratios by visual inspection. From this, they derived the distribution of spheroid-to-disk ratios, as a function of absolute magnitude, and found the overall spheroid-to-disk ratio to be higher in high density environments (galaxy clusters) than in low density environments (the “field”). Schechter & Dressler (1987) found that disks appear to contribute roughly twice as much as spheroids to the mean luminosity density of the Universe. Since a large fraction of the disk light comes from a relatively small number of young stars, Schechter & Dressler (1987) concluded that the relative contribution of spheroid and disk components to the mean stellar mass density of the Universe is very nearly equal.

More recently, Benson et al. (2002) developed a quantitative method to determine galaxy morphology, specifically to estimate spheroid-to-total (S/T) light ratios. This method is implemented in the code GALACTICA (GALaxy Automated Component Image Construction Algorithm). Benson et al. (2002) analyzed a magnitude-limited sample of ~ 100 field galaxies brighter than $I = 16.0$ and found the luminosity functions of spheroids and disks to be remarkably similar. They provisionally concluded that spheroids and disks contribute almost equally to the total stellar mass density in the Universe but stressed the significant uncertainties in their result arising from the small sample size. A larger sample of 1800 galaxies drawn from the Sloan Digital Sky Survey (SDSS; Stoughton et al. 2002) was analyzed by Tasca & White (2005) using the publicly available code GIM2D. They found that $54 \pm 2\%$ of the local cosmic luminosity density in both r and i bands comes from disks, $32 \pm 2\%$ from “pure bulge” systems and the remaining $14 \pm 2\%$ from bulges in galaxies with detectable disks.

In this paper, we perform spheroid/disk decompositions from r -band images of a much larger sample of galaxies in the SDSS. The structure of the paper is as follows. In §2, we describe our dataset and how it is processed. In §3, we present results from the spheroid/disk decomposition. In §4, we derive the luminosity functions of disks and spheroids, and present stellar mass functions and also the supermassive black hole mass function. Finally, in §5, we give our conclusions. Appendices describe extensive tests of the reliability of both GALACTICA and GIM2D (Appendix A), technicalities of the fitting process (Appendix B) and comparisons of our S/T ratio morphologies with more traditional morphological measures (Appendix C). A cosmological model with $\Omega_0 = 0.3$, $\Lambda_0 = 0.7$ is adopted throughout and the Hubble constant is defined to be $H_0 = 100h \text{ km s}^{-1} \text{ Mpc}^{-1}$.

2 DATA: SLOAN DIGITAL SKY SURVEY

2.1 Basic properties

The Sloan Digital Sky Survey (SDSS) is the largest imaging and spectroscopic survey to date. The SDSS Early Data Release (EDR), made publicly available in 2001, consists of a 462 square degree area imaged in five passbands (u, g, r, i and z) and also covered spectroscopically. The SDSS EDR

galaxy catalogue is spectroscopically complete down to $r = 17.7$ and contains measurements of various galaxy parameters (Stoughton et al. 2002). The imaging data were taken with a dedicated 2.5m telescope in the drift-scan (time-delay) integration mode with an effective exposure time of 54s. The data used in this study are the r -band imaging frames with corrections for bias, flat field, cosmic ray and pixel defects (Lupton et al. 2001). Each imaging frame is a 2048×1489 pixel array with a pixel size of $0.394''$.

2.2 SDSS apparent magnitude limit

Benson et al. (2002) measured spheroid-to-total (S/T) light ratios for the field galaxy sample of Gardner et al. (1996) using I -band imaging. The data were originally obtained to determine the K -band luminosity function and Benson et al. (2002) showed that they could be used reliably to estimate S/T ratios for galaxies brighter than $I_{\text{Gar}} = 16.0$ with an rms accuracy of $\sigma_{\text{rms}} \sim 0.1$. Unfortunately, the area covered by this sample is rather small (4.4 deg^2).

The SDSS imaging data were obtained with a larger telescope but using shorter exposure times than those of Gardner et al. (1996). From Monte-Carlo simulations, Benson et al. (2002) established the signal-to-noise required to obtain reliable measurements of S/T using the GALACTICA decomposition code. Assuming that, when applied to the SDSS data, the code will be reliable to the same overall signal-to-noise level, we find that the limiting magnitude required for our SDSS sample is $I_{\text{SDSS}} - I_{\text{Gar}} = 0.4$. Using the mean galaxy colours of Fukugita et al. (1995), the transformation between the I_{SDSS} and r bands is $r - I_{\text{SDSS}} = 0.9$, making the total difference equal to $r - I_{\text{Gar}} = 1.3$ magnitudes. We therefore select EDR galaxies with $r \leq 17.3$ —this is 1.4 magnitudes fainter than the sample used in a similar study by Tasca & White (2006).

2.3 SDSS data selection and galaxy catalogue

Galaxies with $r \leq 17.3$ in the SDSS EDR equatorial strip are plotted in Fig. 1, colour-coded according to the SDSS run number (94, 125, 752 and 756). The black points represent imaging taken in ‘poor’ seeing conditions ($\text{PSF}_{\text{FWHM}} > 1.55''$, where PSF_{FWHM} is the full-width at half-maximum of the point spread function). This cut on of the seeing is used to impose a second galaxy selection criterion since reliable spheroid-to-disk decompositions require that the seeing be less than a typical galaxy half-light radius (Beijersbergen et al. 1999).

The final galaxy selection criterion is redshift. To avoid contamination of the measured redshift by the local galaxy infall velocity, a low redshift cut, $z = 0.02$, is imposed. Since the total SDSS sample begins to tail off at large distance, a high redshift cut, $z = 0.3$, was also imposed.

The selection leads to a total of 8839 SDSS EDR galaxies.

2.4 Sample solid angle

To calculate the solid angle covered by our sample, the galaxy coordinates were accumulated in 0.2° bins. All the

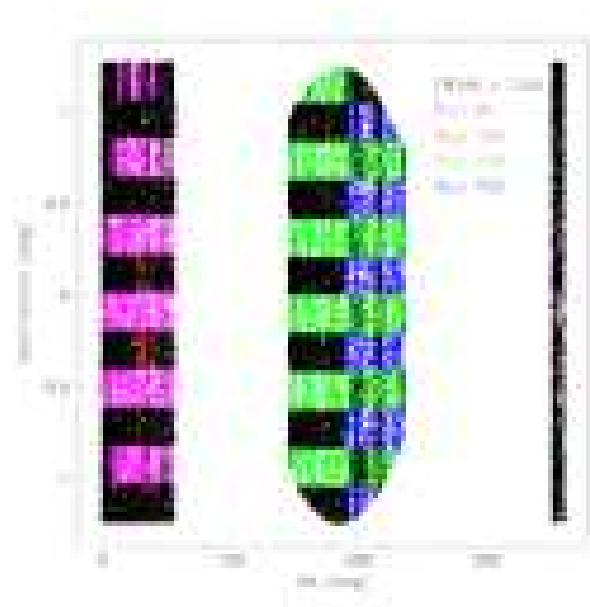


Figure 1. SDSS galaxies that meet our selection criteria. Black points correspond to galaxies imaged when the seeing was greater than $1.55''$.

areas which contain at least one galaxy residing in a particular bin were summed to give the total solid angle. The bin size was chosen such that the derived solid angle was insensitive to small changes in the bin size. As an additional check, this same bin size was used to reproduce the SA of the entire SDSS EDR. For our chosen bin size, the solid angle subtended by our sample is 165.5 square degrees.

2.5 Object detection and astrometry

Object detection was performed using `SEXTRACTOR` v2.2.2 (Bertin & Arnouts 1996). The `SEXTRACTOR` world coordinates of the object centroid positions (x, y) were used to identify the catalogued galaxies within the SDSS frames. The `GALACTICA` code (Appendix A2.3) was run on the extracted postage stamps whose size was set equal to $(2 \times R_p) \times (2 \times R_p)$, where R_p is the Petrosian radius (Lupton et al. 2001). This is large enough to contain many background pixels but sufficiently small to ensure a reasonable convergence time for the fitting procedure. Prior to decomposition, the `SEXTRACTOR` estimate of the local sky background was subtracted from every postage-stamp to ensure that the background level was close to zero (see Appendix A).

2.6 SDSS point spread function (PSF)

Before beginning the decomposition procedure, it is necessary to ensure that the PSF analytic model assumed by the `GALACTICA` code (Appendix A2.3) is a realistic representation of the SDSS PSF. To demonstrate that the SDSS stars are well represented by the analytic Moffat profile assumed by the `GALACTICA` code, the `IRAF` task `IMEXAMINE` was used to fit radial Moffat profiles to a sample of stars imaged on different SDSS frames and at different positions within every frame. Fig. 2 shows radial fits to stellar light profiles

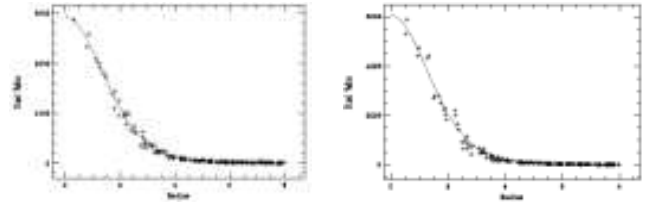


Figure 2. The radial Moffat profile ($\beta = 4.5$) fits (solid line) to the SDSS stellar light profiles (points) for stars found at various positions within several SDSS frames. The radius is in pixels and the Pixel Value are counts. Results are shown for two different frames.

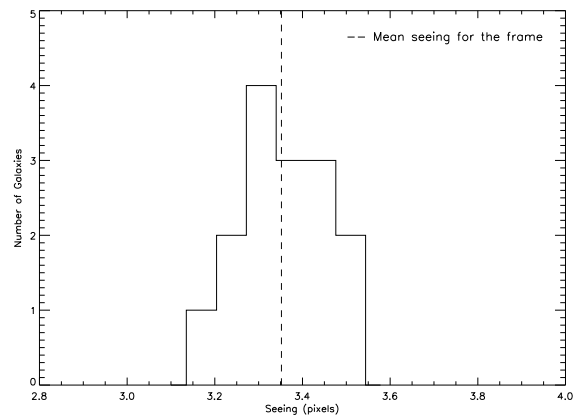


Figure 3. The variation of the PSF across an SDSS frame. The dashed line represents the mean value of the seeing for the frame. The seeing appears not to vary by more than $\pm 5\%$ from the mean value. A similar inspection of other frames shows this to be true in general.

obtained using $\beta = 4.5$ and demonstrates that a Moffat star with this value of β is a good analytic representation of the SDSS PSF.

2.6.1 PSF variation

The `GALACTICA` code assumes a starting value for the PSF equal to the measured value of the seeing in the SDSS and allows the value to fluctuate by $\pm 5\%$ (Appendix A2.3). The $\pm 5\%$ variation is set from the observed variation of the seeing across a typical SDSS frame, as shown in Fig. 3, which demonstrates that for stars imaged at various positions in a given SDSS frame, the FWHM does not change by more than $\pm 5\%$. `GALACTICA` assumes a circularly symmetric PSF, although this may not be precisely true for drift scan observations such as those of the SDSS (Berstein & Jarvis 2002).

The small allowed change in the seeing ensures that the `GALACTICA` code can find the representative value of the seeing at each galaxy position. However, it is important to test how consistently the `GALACTICA` code recovers the ‘correct’ representative PSF for a given galaxy and quantify the effect this has on the recovered S/T ratios. The observed galaxy properties are expected to vary little between the r and i bands but the PSF signatures for these observations will be somewhat different. Fig. 4 shows a good correlation

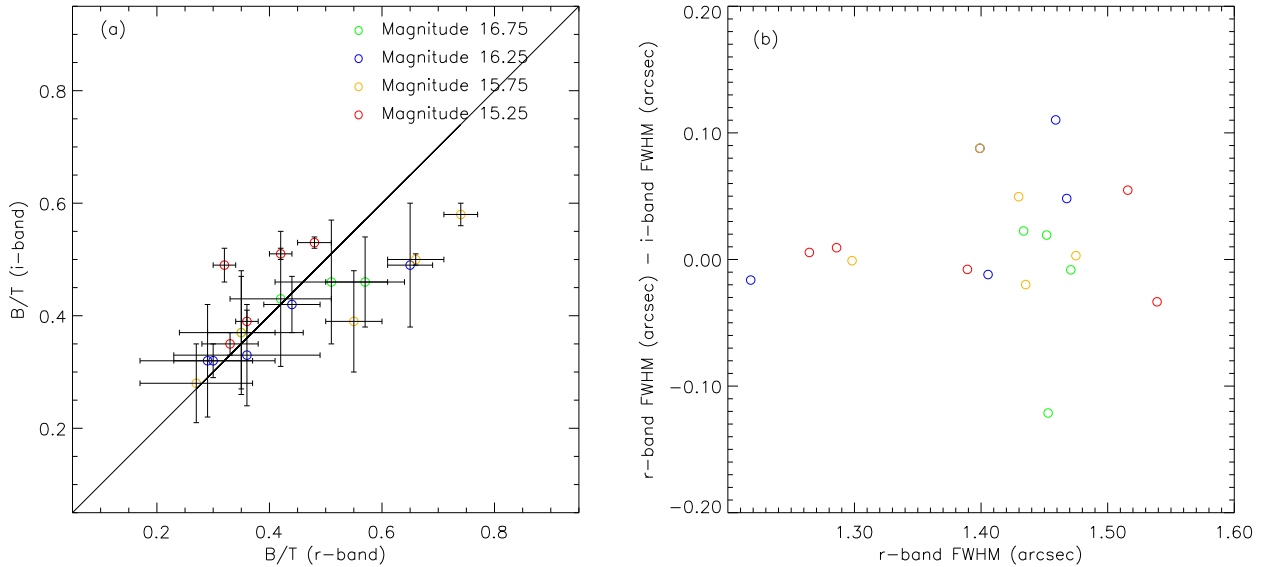


Figure 4. (a) Correlation between S/T ratios obtained for the same galaxies in the r and i bands. The good correlation demonstrates that the S/T ratios are accurately determined for different representative PSFs and across the apparent magnitude range. The recovered S/T ratios show no obvious dependence on galaxy apparent magnitude, indicating that the decompositions are not affected by the variation in the signal-to-noise ratio. (b) The difference in the output GALACTICA seeing for the same set of galaxies observed in the r and i bands. The lack of a trend demonstrates that the GALACTICA code recovers the representative PSF for each galaxy well, without biasing the recovered S/T ratios.

between the S/T ratios obtained for the same set of galaxies imaged in the two bands. The code finds consistent S/T ratios across a range of apparent magnitudes independently of the seeing. Error bars are obtained from 30 Monte Carlo realizations of each of the model fits, assuming the noise appropriate to each image.

3 GALACTICA DECOMPOSITIONS AND GALAXY MORPHOLOGIES

3.1 GALACTICA decomposition outputs

Fig. 5 demonstrates a typical fit to a galaxy light profile. The figure shows the postage-stamp of a real galaxy, a noise-free model generated from the best-fit parameters, along with the individual model disk and spheroid components. In this study, a galaxy is deemed to be sufficiently well represented by the model if the χ^2 per degree of freedom satisfies $\chi^2_\nu < 2.0$, and if there are no obvious structures left in the residual image. Obviously for well-fit data and correctly estimate noise χ^2_ν should be very close to unity. Allowing for larger values of χ^2_ν allows galaxies with small (yet significant) departures from our photometric model to be included in our final sample. An example of a well fit galaxy is shown in Fig. 6. The cross-hatched areas represent potential contamination from overlapping objects as determined by the GALACTICA masking procedure (see Appendix A2.3) and are excluded from the fitting. The inset in Fig. 6 shows a histogram of $dP/d(S/T)$ —the distribution of the spheroid-to-total ratio from 30 Monte Carlo realizations, with the vertical dashed line indicating the best-fit S/T value for this galaxy.

$$S/T = 0.30 \pm 0.07$$

Figure 5. Top: real (left) and model (right) images. Bottom: disk (left) and spheroid (right) component fits. The cross-hatched regions represent potential contamination from overlapping objects (or regions where data were unavailable after the image was re-centred by GALACTICA) and are excluded from the fitting. The contours indicate the pixel values in ADU/s.

3.2 Correlations of S/T with other fit parameters

Understanding the properties of this large statistical sample of galaxies is important since it may reveal features which

$$S/T = 0.30 \pm 0.07$$

Figure 6. Real (left) and residual (right) images. The inset shows the distribution of S/T ratios from 30 Monte Carlo realizations with the vertical dashed line indicating the best-fit S/T. The value of χ^2_{ν} is acceptably small and the residual image also shows a good fit to the data.

otherwise would not be discovered in smaller samples such as those discussed in Appendix C. Equally, any unexpected correlations between parameters could help discover and reduce possible biases introduced by the fitting routine.

Histograms of various properties of our SDSS galaxies inferred from the GALACTICA decompositions are shown in Fig. 7. These plots reveal the following:

- (i) a large number of highly elliptical spheroids;
- (ii) an excess in the number of galaxies with spheroid position angle, θ_s , equal to 0° and 180° ; and,
- (iii) a non-uniform distribution of the cosine of the disks' inclination, $\cos(i)$.

In the remainder of this section, we explore the possible origins of these unexpected distributions and their influence on the recovered values of the S/T ratio.

3.2.1 S/T vs. Ellipticity

Around 15% of galaxies appear to have a highly elliptical spheroid component whose ellipticity has reached the imposed upper limit² of $e = 0.83$. A large number of frames have been inspected by eye and show that these galaxies generally exhibit bar-like structures in the direction of the detected highly elongated spheroidal component. In these cases, the existence of this extra component, which is not part of the fitted model, drives the code to fit small and highly elliptical spheroids (Fig. 8). While in principle it is possible to include additional components, such as bars, in the photometric model (see, for example, Gadotti & Kauffmann 2007) we have not done so here due both to the fact that fitting them would result in prohibitively long times to fit each image and that, for poorly resolved galaxies, additional components can cause further systematic errors such as the one described above. These galaxies are generally disk-dominated (with mean S/T ratio of 0.14) and thus we expect this shortcoming of the model to introduce only a small bias on the overall S/T ratio. (It should be noted, however, that this problem may be occurring even in cases

² The upper limit for the ellipticity corresponds approximately to that of the most elliptical observed galaxies (Lambas, Maddox & Loveday 1992).

$$S/T = 0.37$$

Figure 8. An example of a galaxy with a highly elliptical spheroid. This galaxy demonstrates how the central bar-like structure in the galaxy results in the detection of a highly elliptical spheroid along the same direction. The top row shows the real (left) and model (right) images. The middle row shows the disk (left) and spheroidal (right) components. The bottom row shows the real (left) and residual (right) images.

where the fitted ellipticity is less than 0.83 if seeing has made the bar component appear rounder.) Any bias that is introduced would increase this ratio, resulting in a slight overestimation of the spheroid luminosity density in §4.

Similar problems of this type (i.e. fitting of additional photometric components of galaxies such as bars or isophotal twists by a component of the photometric model) have been noted and discussed by Tasca & White (2006) and Simard et al. (2002). In such cases, the S/T ratio will be incorrectly estimated. We return to this problem in §4.

3.2.2 S/T vs. spheroid position angle

Many galaxies appear to have $\theta_s \sim 0^\circ$ (or, equivalently, $\theta_s \sim 180^\circ$). This could be due to either:

- (i) some feature intrinsic to the code such as the initial estimate of θ_s ; or,
- (ii) a feature intrinsic to the data.

Such a biased distribution does not arise when fitting mock images constructed either internally by GALACTICA or ex-

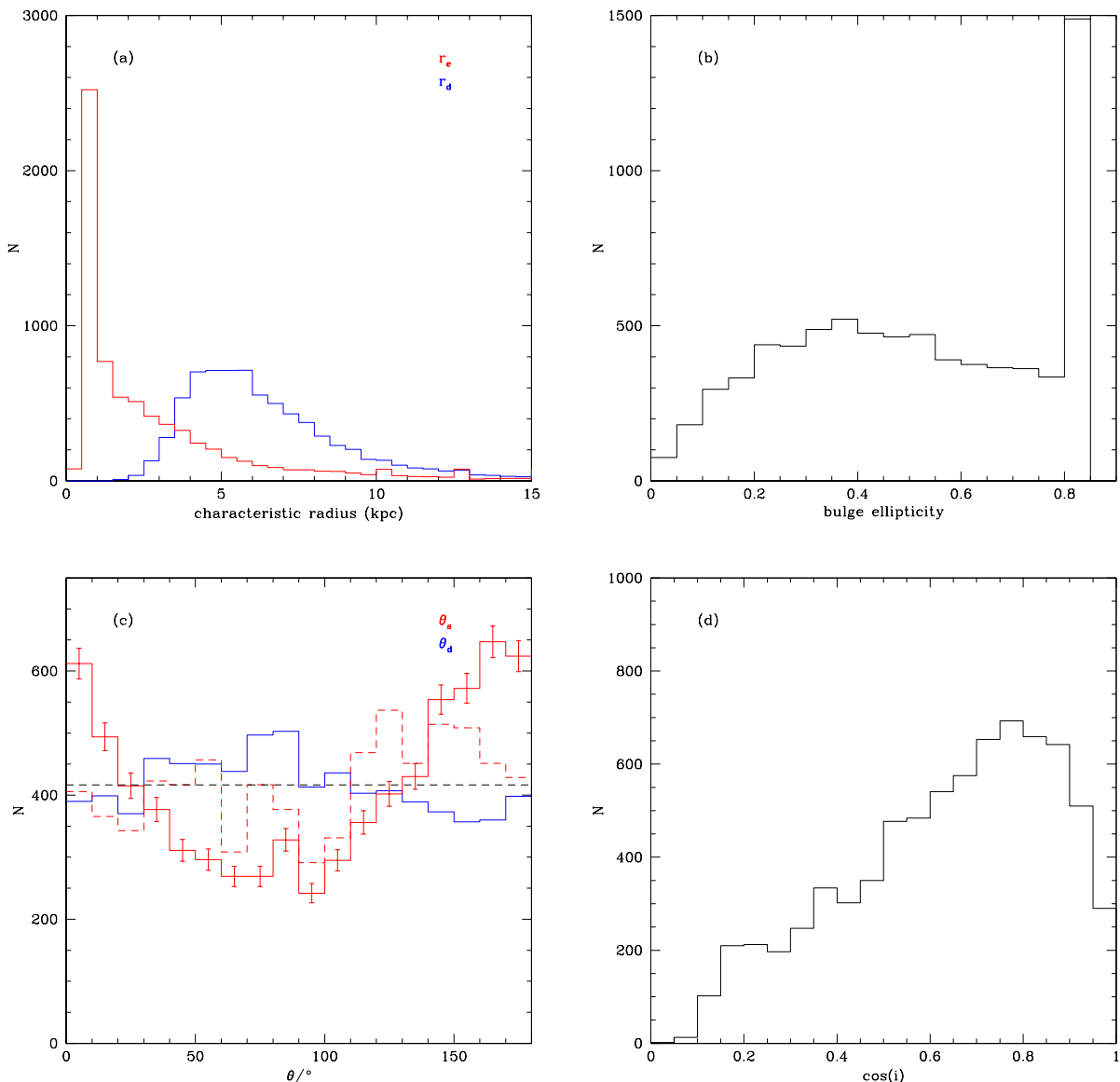
$\chi^2 < 2$; 7493/8839 galaxies

Figure 7. Histograms of parameters recovered by GALACTICA from our sample of SDSS galaxies. a) Characteristic sizes of the spheroidal and disk components. b) Ellipticity of the spheroidal components. c) Position angles of disks and spheroids. The dashed histogram shows the position angles of well resolved spheroids (those with effective radii greater than three times the PSF FWHM). d) Cosine of the inclination angle of the disks. Where appropriate, spheroids are represented in red and disks in blue.

ternally by IRAF (see Appendix A3.2 for details of these tests), suggesting that (i) is not the correct explanation.

Explanation (i) can, in fact, be ruled out by rotating the images by some angle prior to fitting. If the problem were intrinsic to the code, we would expect to see no change in the distribution of θ_s . In fact, when we rotate the images by 90° , we find that the distribution of θ_s is shifted by 90° (see Fig. 9), indicating that it is some feature of the images themselves that is causing this problem. The same is true if we instead rotate galaxies by 45° . (Note that, in the case of a 45° rotation we crop to the largest square which fits within the rotated image. As a result, there are fewer pixels available to fit and therefore larger errors in the fit param-

eters.) Point (ii) is a plausible explanation since the data were taken in drift-scan mode along the easterly direction which corresponds to $\theta = 0^\circ$. This can lead to small asymmetries in the actual PSF (Bernstein & Jarvis 2002). Since we are using a circularly symmetric PSF in our photometric model, GALACTICA may try to fit slightly elliptical bulges with $\theta_s \approx 0^\circ$ to match the actual PSF shape. Note that, as expected, for well-resolved spheroids, the distribution of θ_s is close to uniform (dashed histogram in the lower-left panel of Fig. 7).

For our purposes, the crucial issue is whether the bias in θ_s affects the derived S/T. To quantify the effects of this bias on the recovered S/T ratio, we re-fit a sample of our images

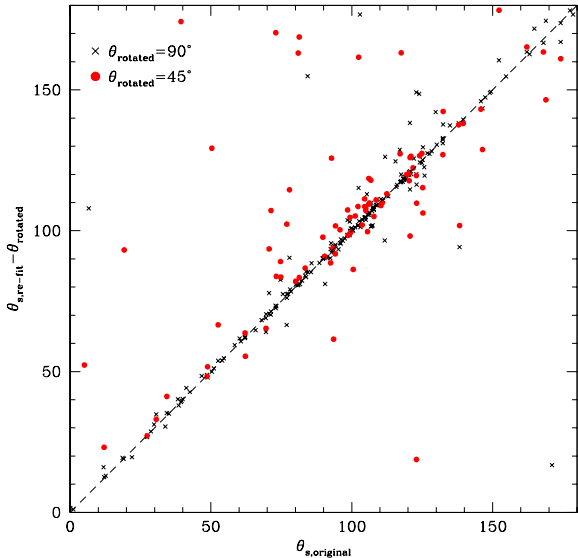


Figure 9. A comparison of the bulge position angles recovered for a sample of ~ 100 SDSS galaxies fit before (x-axis) and after (y-axis) rotation by $\theta_{\text{rotated}} = 45^\circ$ and 90° . When rotating images by 45° we crop them to the largest square which fits entirely within the rotated image. As a result there are fewer pixels to fit and therefore a larger scatter in θ_s values recovered.

keeping θ_s equal to θ_d (i.e. we did not allow the spheroid position angle to vary freely). We find that the S/T ratios recovered correlate extremely well with those found with θ_s as a free parameter, with scatter consistent with the fitting uncertainties in S/T (see the left-hand panel of Fig. 10). An excellent correlation is also found if we rotate our images by 45° (right hand panel of Fig. 10). The larger scatter in this case is caused by the reduced number of pixels available for fitting in our rotated images. We conclude that this bias in the distribution of θ_s does not affect our estimates of S/T. We have further found that the bias in the distribution of θ_s is strongest for poorly resolved, low ellipticity spheroids. For larger spheroids, particularly those which are quite elliptical, there is no apparent bias.

In conclusion, the bias in θ_s seems to be due to some feature intrinsic to the data, perhaps an asymmetry in the PSF due to the observing method. We do not believe that this bias affects the recovered S/T ratios at any significant level since re-fitting the images with the bulge position angle locked to equal that of the disk (which is essentially unbiased—see Fig. 7) does not significantly alter the S/T ratio in the vast majority of cases.

3.2.3 S/T vs. disk inclination

A large number of objects in the sky which are randomly inclined to the line-of-sight should have a uniform distribution of $\cos(i)$. Fig. 7 clearly shows that this is not the case for the inclination angles of the disk components obtained by decomposing our sample of SDSS galaxies.

To test whether the apparently incorrect recovery of the disk inclination is an artifact of the fitting procedure, a sample of 200 mock galaxies was generated using the GALACTICA

code (see Appendix A). The S/T ratios were chosen at random in the interval $[0, 1]$. The remaining parameters, including the value of $\cos(i)$, were also chosen at random. Fig. 13 demonstrates that the GALACTICA code generally recovers the $\cos(i)$ distribution for 200 model galaxies quite well. However, a noticeable feature is a slight deficit at $i = 90^\circ$ and a corresponding at $i \sim 75 - 80^\circ$. This excess reflects the fact that fits avoid the 90° limit since this would correspond to fitting an infinitely thin edge-on disk and, because of seeing, the disks are never infinitely thin edge-on. (The feature remains even if the allowed inclination range is increased from $[0^\circ, 90^\circ]$ to $[-180^\circ, 180^\circ]$.) The S/T ratios are not affected by this problem, i.e. model galaxies with input value $i \sim 90^\circ$ but recovered value $i \sim 85^\circ$ show no bias in the recovered S/T ratio.

Such biases in the distribution of $\cos(i)$ have been seen in other studies employing 2D galaxy decomposition techniques (see, for example, Simard et al. 2002; Tasca & White 2006) and can occur because the fitting codes tend to fit disk components to radial variations in axial ratio or position angle in spheroids (Simard et al. 2002). Tasca & White (2006) used GIM2D to fit the 2D images of galaxies in the SDSS. They found a biased distribution of $\cos(i)$, with intrinsically brighter galaxies showing the most biased distribution. Fig. 11 reproduces Fig. 10 of Tasca & White (2006), with results from this work overlaid. Our results, using the same dataset but a different galaxy decomposition code, are in excellent agreement with those of Tasca & White (2006).

Allen et al. (2006) performed 2D galaxy decompositions, also using GIM2D, on galaxies in the Millennium Galaxy Catalogue and found that disk-dominated galaxies ($S/T < 0.8$) had a more uniform (although still biased) distribution of $\cos(i)$. Fig. 12 reproduces their results, with comparable results from our own work overlaid. In this case, we find the opposite trend: our $\cos(i)$ distribution is more uniform for the $S/T > 0.8$ sample, although the errors are large. We find that galaxies must have angular sizes of several times the seeing half-width at half-maximum in order for the inclination to be well constrained. From Fig. 1 of Allen et al. (2006), we would therefore conclude that a large fraction of their galaxies should have poorly constrained inclinations.

Assuming that the bias in $\cos i$ arises due to GALACTICA using the disk component of the photometric model to fit radial variations in the spheroid, it is possible to make an approximate correction for this bias. Such a correction was developed by Tasca & White (2006). In §4.3 we will employ their correction, and a similar yet more detailed correction to assess the impact of this bias on our results.

3.2.4 Effects of fitting Sérsic index

We have chosen not to include the Sérsic index as a free parameter in our photometric model, instead holding it fixed at $n = 4$ (corresponding to a de Vaucouler’s profile). Tasca & White (2006) demonstrated that $n = 4$ provides a good fit to the majority of spheroids in a magnitude limited sample, and that there is a very good correlation between the values of S/T obtained using fixed $n = 4$ and free n fits. To examine this in our own data we fit a subsample of our galaxies allowing n to vary. In Fig. 14 we show the recovered S/T ratios assuming a de Vaucouler’s profile (x-axis) and a

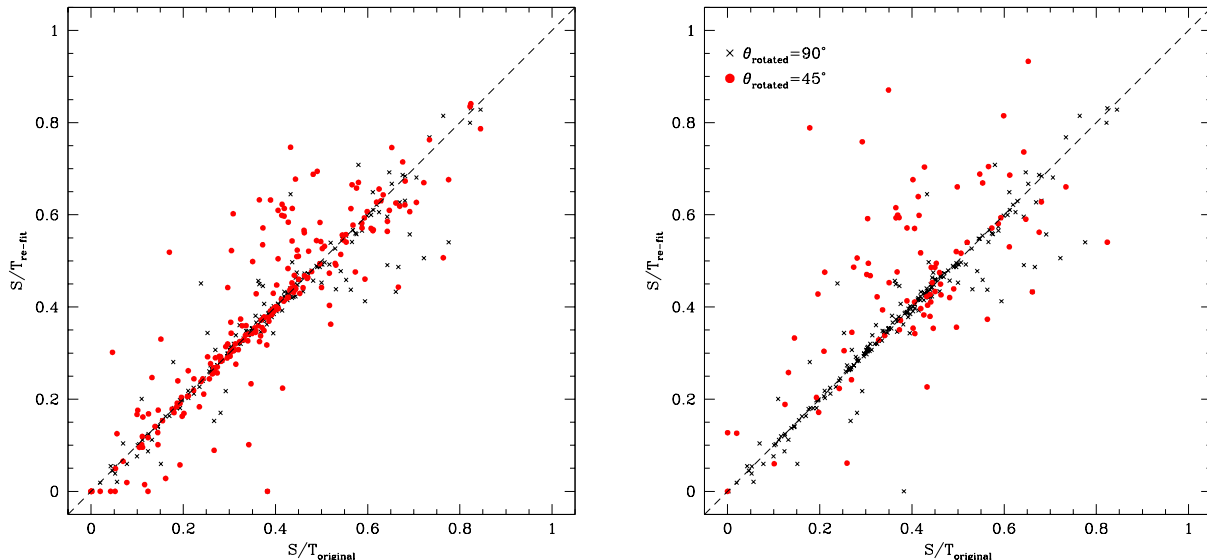


Figure 10. *Left panel:* Comparison of estimates of S/T for a sample of ~ 100 SDSS galaxies estimated from the actual image and from the image rotated anticlockwise by 90° (black crosses). Also shown are the results of re-fitting these images with the spheroid position angle forced to equal the position angle of the disk (red circles). *Right panel:* Comparison of estimates of S/T for the same sample estimated from the actual image and from the image rotated anticlockwise by 90° (black crosses) and by 45° (red circles). When rotating images by 45° we crop them to the largest square which fits entirely within the rotated image. As a result there are fewer pixels to fit and therefore a larger scatter in S/T values recovered.

Sérsic profile (y-axis). There is a good correlation between the results obtained using de Vaucouler’s and Sérsic profiles. This is particularly true when $n \gtrsim 2.5$. For lower values of n (blue points in Fig. 14) we see some large discrepancies. These occur for galaxies which had a low S/T in the de Vaucouler’s fit, but are given a high S/T when fit by a Sérsic profile. Of course, for $n \approx 1$ there is no difference in our photometric model between disks and spheroids (except for the fact that disks may be highly inclined to the line-of-sight while spheroids are limited in how elliptical they may become). It is not surprising therefore that GALACTICA mixes disk light between the two model components in such cases. We find that, when allowing the Sérsic index to be fit as a free parameter the fraction of light emitted by disks (averaged over all galaxies in our sub-sample using a $1/V_{\max}$ weighting) decreases from 60% to 52%. This effect is very similar to that found by Tasca & White (2006). We consider this to be a lower limit on the disk light fraction since, as discussed above, for some galaxies a fraction of the disk light will have been fit by a spheroidal component with $n \approx 1$.

4 LUMINOSITY AND MASS FUNCTIONS

4.1 Introduction

The spatial abundance of galaxies is expressed by means of the luminosity function (LF), defined as:

$$dn(M) = \phi(M)M, \quad (1)$$

where dn is the number density of galaxies with absolute magnitude in the range $M, M + \Delta M$. The simplest way to calculate the luminosity function is using the $1/V_{\max}$ method

in which the number of galaxies in each individual absolute magnitude bin is divided by the volume of space that has been surveyed at that magnitude. Galaxies in any given absolute magnitude range are assumed to be uniformly distributed in the surveyed volume which is not the case if any local overdensities are present. Maximum likelihood techniques circumvent this problem and provide more accurate estimates of the luminosity function. Here, we will employ the $1/V_{\max}$ as well as the Stepwise Maximum Likelihood (SWML) non-parametric estimator (Efstathiou, Ellis & Peterson 1988) which characterizes the LF as a series of steps. We will also employ the STY parametric estimator (Sandage, Tammann & Yahil 1979), assuming a Schechter (1976) functional form

$$\phi(M) = 0.4 \ln 10 \phi_* 10^{-0.4(M-M_*)(\alpha+1)} \exp[-10^{-0.4(M-M_*)}], \quad (2)$$

where M_* is a characteristic magnitude, α is the faint-end slope and ϕ_* is the normalization. Integrating over the Schechter function provides an estimate of the luminosity density. This can also be obtained by summing up all the individual SWML contributions.

Computing the spheroid and disk LFs is more complicated since there is an additional constraint to be considered (Benson et al. 2002), namely the detectability of a spheroid/disk depends both on the component’s apparent magnitude and on the corresponding S/T . This needs to be accounted for when constructing the luminosity function. A detailed discussion of the application of these methods can be found in Benson et al. (2002). We use exactly the same methods as (Benson et al. 2002) to estimate luminosity functions from our present dataset.

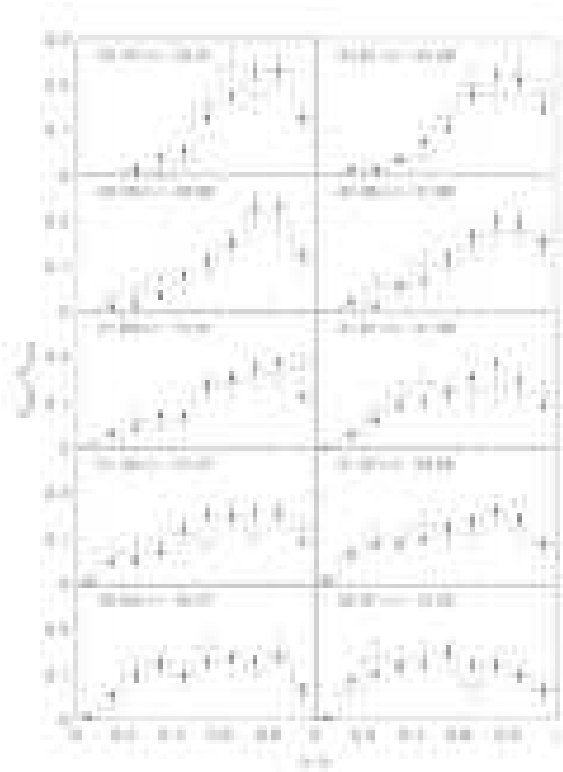


Figure 11. The distribution of axial ratio b/a (equivalent to $\cos i$) as a function of galaxy luminosity. Histograms show results from Tasca & White (2006) (this figure is a reproduction of their Fig. 10), while points show results from this work. Both datasets show that the bias in $\cos i$ occurs primarily for the most luminous galaxies.

Benson et al. (2002) used a functional form for STY parametric fits to the spheroid and disk LFs which had a Schechter \times exponential form. We find that the functional form of Benson et al. does not provide a good description of our larger sample of galaxies. We have been unable to find a suitable functional form which does provide a good description and so have not performed STY fits to the spheroid and disk luminosity function data.

4.2 SDSS absolute magnitudes and K+E corrections

In order to estimate the luminosity function, we require galaxy absolute magnitudes. A galaxy at redshift z , with apparent magnitude m , has an absolute magnitude M given by:

$$m - M = 25 + 5 \log_{10}(D_L) + \text{KE}(z) \quad (3)$$

where D_L is the luminosity distance in megaparsecs and $\text{KE}(z)$ is the K+E correction.

K+E corrections for our catalogued galaxies were obtained using a code kindly provided by Carlton Baugh. It employs the revised isochrone stellar population synthesis models of Bruzual & Charlot (1993) to determine present-day galaxy luminosities. The model assumes a stellar initial mass function (IMF) and a star-formation rate

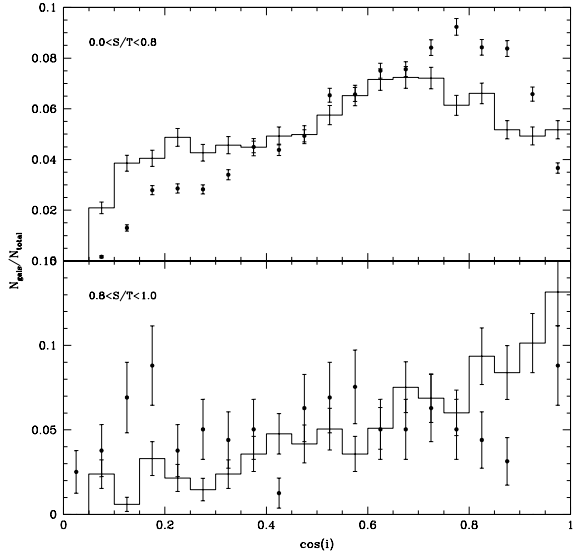


Figure 12. The distribution of $\cos i$ split by S/T. Histograms show results from Allen et al. (2006) (this figure is a reproduction of their Fig. 9), while points show results from this work. While both datasets show biased distributions of $\cos i$, the trends with S/T appear to differ, with the Allen et al. (2006) dataset showing a more uniform distribution of $\cos i$ for galaxies with low S/T.

$\psi(t) \propto \exp(-t/\tau)$, with timescale, τ . A grid of models was generated by varying the metallicity and τ . We assume a Salpeter (1955) IMF and apply a simple dust extinction law. At every point on the grid, a table of absolute magnitudes, galaxy colours, K+E corrections and galaxy stellar mass-to-light ratio is generated. The model that best matches the observed $g - r$ and $r - i$ colours of each galaxy is then used to infer its present-day ($z = 0$) r -band absolute luminosity, K+E correction and stellar mass-to-light ratio. The mass-to-light ratio is used to convert luminosities to stellar masses in order to estimate stellar mass functions (see §4.5). Note that the K+E corrections are based on the total (i.e. spheroid plus disk) colour of a galaxy.

4.3 Luminosity function estimates

We estimate luminosity functions using the methods described in detail by Benson et al. (2002) and employ both the SWML and $1/V_{\text{max}}$ estimators (for the total luminosity function we also employ the STY estimator). We estimate the luminosity functions of spheroids and disks, as well as the total galaxy luminosity function for our sample of SDSS EDR galaxies.

As noted in Appendix B2, our requirement that images be reasonably well fit by GALACTICA (i.e. $\chi^2_\nu < 2$) introduces some bias in both the apparent magnitude and redshift distributions of our galaxy sample. To correct this bias we make the assumption that the distribution of S/T for galaxies with $\chi^2_\nu > 2$ is the same as that for galaxies of comparable apparent magnitude and redshift and with $\chi^2_\nu < 2$. Such an assumption may of course not be correct, for example if disk-dominated galaxies are more likely to be poorly described by our photometric model. Nevertheless,

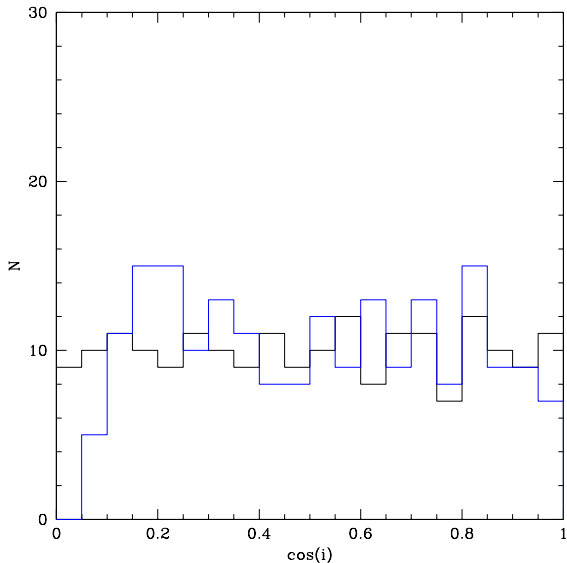


Figure 13. The input (black) and the recovered (blue) $\cos(i)$ distribution for 200 model galaxies created and decomposed using the GALACTICA code. The figure demonstrates that the non-uniformity in the $\cos(i)$ is not caused by the fitting code. An apparent excess of galaxies with $i \sim 75 - 80^\circ$ can be seen.

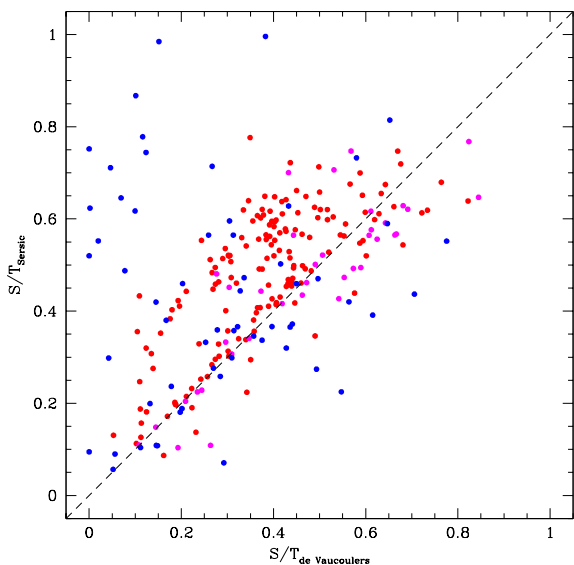


Figure 14. The S/T ratios measured for a subsample of our galaxies. On the x-axis we plot the value obtained assuming a de Vaucouleurs’s profile for the spheroid (i.e. a Sérsic profile with fixed $n = 4$) while on the y-axis we show the results of fits in which we allow the Sérsic index n to vary. Red points show galaxies for which the best fit $n > 4$, magenta points show galaxies for which $2.5 < n \leq 4$ while blue points show galaxies with $n \leq 2.5$.

this assumption represents the simplest correction that can be made for the bias. Therefore, for each galaxy with $\chi^2_\nu > 2$ we identify all well-fit galaxies with apparent magnitude differing by less than 0.1 and redshift differing by less than 0.03 from the true values for the poorly-fit galaxy. We then select a galaxy from this sample at random and adopt its S/T ratio for our poorly-fit galaxy.

In Appendix A3.2 we find that the value of S/T recovered by GALACTICA (and also GIM2D) for mock images are biased. The median bias in S/T produced by GALACTICA can be approximated by a linear dependence on the true S/T (see Fig. A6). We use this linear relation to apply a correction to the value of S/T recovered for each SDSS galaxy in order to obtain an estimate of the unbiased value. We use these corrected estimates of the S/T when estimating luminosity and mass functions.

We find that there are only small changes in the measured luminosity functions, the most significant being a small enhancement in the abundance of bright spheroids. The luminosity density ratio quoted above varies by less than 0.5σ after correcting for this bias.

Our results are displayed in Fig. 15. For galaxies whose images are well-fit by our model, we find that the STY method accurately recovers the parameters of the total luminosity function; furthermore, the STY fit traces the corresponding SWML points very well. The values of M_* and α obtained from the STY fit to the total luminosity function agrees very well with that of Nakamura et al. (2003) (SDSS r -band, $z = 0$). While we have not been able to find a parametric form which fits the spheroid and disk 2D luminosity functions ($\Phi(M, S/T)$) we have determined the parameters of Schechter functions which fit the SWML data points reasonably well. These should not be considered good fits in a statistical sense, merely useful fitting functions. The parameters of the best fit Schechter functions are given in Table 1.

We calculate luminosity densities of disks and spheroids by integrating over the SWML points³. We find the luminosity densities for spheroids and disks to be: $\rho_L = 0.611 \pm 0.008 \times 10^8 h L_\odot \text{ Mpc}^{-3}$ and $\rho_L = 1.07 \pm 0.02 \times 10^8 h L_\odot \text{ Mpc}^{-3}$ respectively.

These values are in contrast with the findings of the previous study of Benson et al. (2002) who found the spheroid and disk luminosity densities to be very nearly equal. Of course, Benson et al. (2002) used a very small sample of galaxies to compute luminosity densities, finding a ratio of disk to spheroid luminosity density of 1.2 ± 0.9 . Our current sample gives a ratio of 1.75 ± 0.04 , which is consistent with that of Benson et al. (2002).

4.3.1 Corrections for Systematic Effects

Tasca & White (2006) propose a method to correct for the bias introduced by the non-uniform $\cos i$ distribution

³ No correction is included for galaxies fainter than the lower limit shown in the figures. Using the best-fit Schechter functions listed in Table 1 we estimate that including fainter spheroids/disks would lead to corrections of 1%/4% respectively. We regard these corrections as speculative since the Schechter function does not provide a good fit to the spheroid and disk luminosity functions.

Table 1. Best fitting Schechter function parameters for luminosity functions of total, spheroid and disk components. For the total luminosity function the best fit parameters are determined using the STY method. For the disk and spheroid luminosity function we instead fit a Schechter function to the non-parametric luminosity function determined using the SWML method—these should be considered useful fitting functions only, not good fits in any statistical sense. For the spheroid and disk luminosity function fits, the maximum deviation from the SWML data points is given in the final column.

Component	$M_* - 5 \log h$	α	$\phi_0/h^3 \text{Mpc}^{-3}$	Max. Dev.
Total	-20.62	-1.19	0.00155	N/A
Spheroid	-20.98	-1.18	0.00348	32%
Disk	-20.40	-1.39	0.00830	27%

discussed in §3.2.3. This method involves using only those galaxies with $\cos i < 0.5$ (which Tasca & White (2006) consider to be true disks) to estimate the fraction of light emitted by disks as a function of absolute magnitude. This function, $f_{\text{disk}}(M_r)$, is then averaged over the total galaxy luminosity function in order to obtain an estimate of the fraction of light emitted by disks. Tasca & White (2006) include a correction for the inclination-dependent dust extinction experienced by galaxy disks, finding that, at any given magnitude, f_{disk} should be 2.56 times⁴ the fraction of light emitted by disks with $\cos i < 0.5$. Figure 16 shows the function f_{disk} for our galaxies. Filled red points are the result of summing the luminosities of disks over all values of $\cos i$, i.e. with no attempt to correct for the biased distribution of $\cos i$. Filled black points show the result after applying the Tasca & White (2006) correction (note that in cases where this correction would imply $f_{\text{disk}} > 1$ we limit the value to unity). Averaging over the SDSS r -band luminosity function of Blanton et al. (2003) we find that $(53 \pm 3)\%$ of the local luminosity density is contributed by disks. This is consistent with the $(54 \pm 2)\%$ obtained by Tasca & White (2006). It should be noted that this result is robust to changes in our decision to include all galaxies with $\chi_\nu^2 < 2$ in our final sample. Reducing this cut to $\chi_\nu^2 < 1.2$ for example results in a disk luminosity fraction of $(47 \pm 3)\%$ —consistent with the previous result within the quoted errors.

We can attempt to use this same approach to construct disk and spheroid luminosity functions corrected for the non-uniform $\cos i$. To do this, we take our catalogue of galaxies and identify those with $\cos i < 0.5$. These galaxies are assumed to have been correctly fitted (i.e. the disk component of our fit corresponds to a real thin disk in these galaxies) and are placed into a refined catalogue. Since we assume that the true $\cos i$ distribution should be uniform we expect one galaxy with $\cos i > 0.5$ for each galaxy with $\cos i < 0.5$. Therefore, for each galaxy in our $\cos i < 0.5$ sample we search for a galaxy with similar spheroid and face-on disk absolute magnitudes but with $\cos i > 0.5$. The most similar galaxy is added to our refined catalogue. At the end of this procedure what remains is a sample of galaxies with $\cos i > 0.5$ for which there are no $\cos i < 0.5$ counterparts. We assume that in these cases the disk component has been used to fit some feature in the spheroid. Therefore, we set the S/T ratio of these remaining galaxies to 1 and include them in our refined catalogue.

⁴ This correction would be precisely 2 if there were no dust-extinction of the galaxy disks.

This procedure should give a conservative lower limit to the disk luminosity fraction. The disk fraction obtained via this method is shown by the blue points in Fig. 16. Note that this matches the Tasca & White (2006) method for bright galaxies, but falls below it at faint magnitudes. The reason for this is simple: the Tasca & White (2006) method assumes that the total disk luminosity in any bin of absolute magnitude is 2.56 times that of disks with $\cos i < 0.5$ in that bin, *even if that exceeds the total fitted disk luminosity of all galaxies in that bin of absolute magnitude*. Thus, the Tasca & White (2006) method can create additional disk light in some bins, contrary to the assumption that the image decomposition code has added in extra disk light to fit details of the spheroid component. The open red circles in Fig. 16 show the fraction of light from disks with $\cos i < 0.5$ while the solid red line indicates the total disk luminosity reduced by a factor 2.56. Where the open red circles lie above the red line the Tasca & White (2006) method must create additional disk light. In our more detailed method, disk light can never be created, and so the blue points always lie below the red points.

The problem just discussed illustrates the limitations of the Tasca & White (2006) method, and indicates that the reality here is significantly more complicated than the simple assumption adopted by Tasca & White (2006). Nevertheless, our more detailed implementation of their method should still give a good lower limit on the disk luminosity fraction. The resulting disk and spheroid luminosity functions are shown as crosses in Fig. 15. We find a disk luminosity fraction of $(43 \pm 1)\%$.

In short, the Tasca & White (2006) method works provided all objects with $\cos i < 0.5$ are correctly fit (i.e. the model disk is fit to a true disk). If this assumption is correct, then our data imply that GALACTICA and GIM2D must be systematically failing to fit the disk components of equivalent galaxies with $\cos i > 0.5$, assigning some of the disk light to a spheroid component. This could occur, for example, if in face on galaxies the codes use the spheroid component to fit a bar feature in the disk.

To summarize, our results suggest that stars in disks contribute between 43 and 64% of the local luminosity density. Tasca & White (2006) found a disk contribution of $54 \pm 2\%$ which is entirely consistent with this range. Furthermore, if we apply Tasca & White’s correction for the bias in $\cos i$ precisely as they did we find a disk fraction of $(53 \pm 3)\%$, in excellent agreement with their result. However, as we have shown above, it is not clear that the Tasca & White (2006) correction is entirely valid and hence we

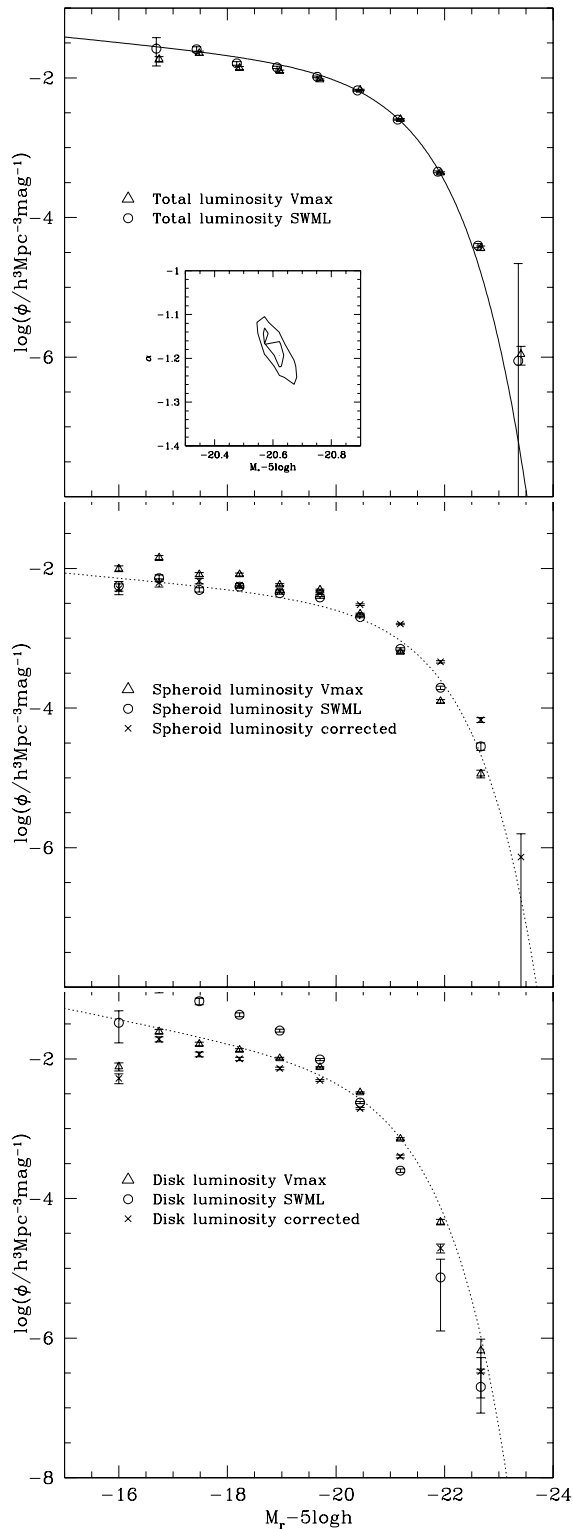


Figure 15. Luminosity functions for our sample of 7493 galaxies with $\chi^2_\nu < 2.0$. Magnitudes are the total absolute magnitudes of the galaxies in the upper panel, and the absolute magnitudes of spheroid and disk components in the lower panels. Open symbols show the $1/V_{\max}$ and SWML estimates, while crosses show the SWML estimate after correcting for the biased distribution of $\cos i$; the solid line in the top panel represents the STY fit, while dotted lines in the lower panels indicate the best fit Schechter function to the SWML data points. The top panel displays the total galaxy luminosity function, the middle panel the luminosity function of spheroids and the lower panel, the luminosity function

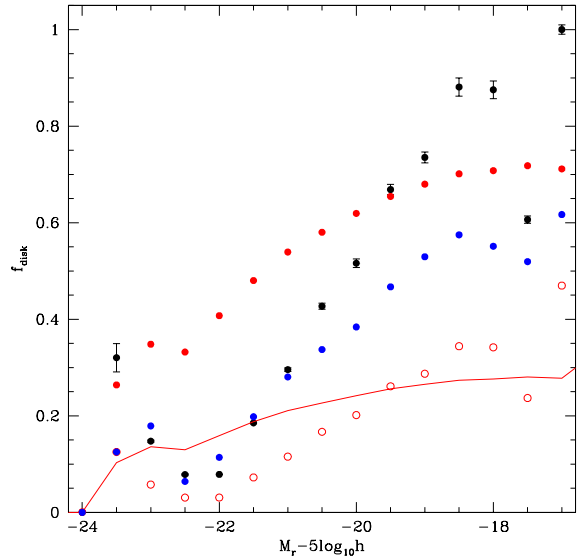


Figure 16. The disk light fraction, f_{disk} , as a function of absolute magnitude. Red points show f_{disk} measured from our image decompositions with no attempt to correct for the non-uniform distribution of $\cos i$. Black points show the disk fraction resulting from the correction described by Tasca & White (2006) (error bars are shown only for these points for clarity—they are similar for other points). Blue points show the result of applying a more detailed correction motivated by the assumptions of Tasca & White (2006). Red open circles indicate the fraction of light in disks with $\cos i < 0.5$, while the red line shows the filled red points reduced by a factor of 2.56.

prefer to quote the range above which we feel is a very conservative estimate of the disk contribution to the luminosity density.

Finally, as noted in §3.2.1, we suspect that GALACTICA frequently uses a highly elliptical spheroid component to fit bar-like features in galaxy disks. If we assume that all spheroids at the upper limit of allowed ellipticities (i.e. those in the final bin in Fig. 7) are in fact bars, and therefore count their light as originating from the disk we find that our estimate of the disk luminosity density is increased by 16% while that of the spheroid luminosity density is decreased by 10%. Consequently, this correction would adjust the disk luminosity density fraction from 43% up to 50%.

4.4 Comparison with theoretical predictions

In Fig. 17 we compare our estimate of the disk and spheroid luminosity functions with predictions from the Baugh et al. (2005) and Bower et al. (2006) implementations of the GALFORM semi-analytic model of galaxy formation. These two models differ in a number of important respects. For example, in Bower et al. (2006) feedback from the emission of active galactic nuclei plays a role in quenching cooling flows in clusters; in the Baugh et al. (2005) model, a top-heavy IMF is assumed for stars that form in starbursts. The two models, however, assume similar mechanisms for the formation of disks and spheroids: disks form when spinning gas cools in a halo while spheroids form either by major mergers or by instabilities in the disks. Although both models

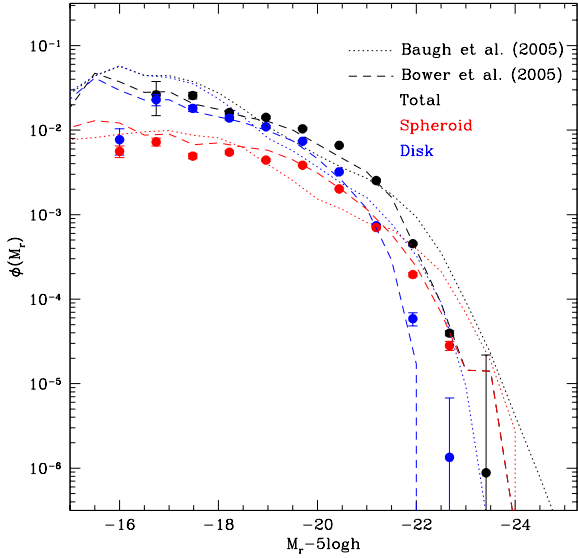


Figure 17. Luminosity functions disk and spheroid and total light (indicated by colour; see legend for details). The symbols show our estimates for SDSS galaxies in this work and the lines two different implementations of the GALFORM semi-analytic model: Baugh et al. (2005) (dotted lines) Bower et al. (2006) (dashed lines).

generally provide a reasonable description of many galaxy properties, they have different strengths and weaknesses. Neither of them has been previously applied to the study of galaxy morphology, although the parameter f_{ellip} (first introduced into semi-analytic models by Kauffmann, White & Guiderdoni (1993)), which controls the mass ratio at which a galaxy merger is deemed to destroy any pre-existing disks and create a spheroid, was constrained to produce a good match to morphological fractions as a function of absolute magnitude and galaxy colours.

Fig. 17 shows that both GALFORM models reproduce the main trends seen in the SDSS luminosity functions. At faint magnitudes, the luminosity function is dominated by disks while at bright magnitudes disks and spheroids make comparable contributions. The Bower et al. (2006) model in particular provides a good match to the SDSS luminosity functions.

4.5 Stellar mass functions

As noted in §4.2, our procedure for determining K+E corrections also provides an estimate of the stellar mass of each galaxy. Using these stellar masses we have constructed total, spheroid and disk stellar mass functions using the SWML and STY (for total mass only) methods. For the spheroid and disk mass functions we also derive the Schechter function which best fits the SWML data points. It should be noted that we implicitly assume that the mass-to-light ratio, Υ , determined for each by our K+E correction procedure is the same for both the disk and spheroid components. In reality, the recovered value of Υ reflects some weighted average of the Υ of each component. To improve upon this situation would require a more advanced procedure in which

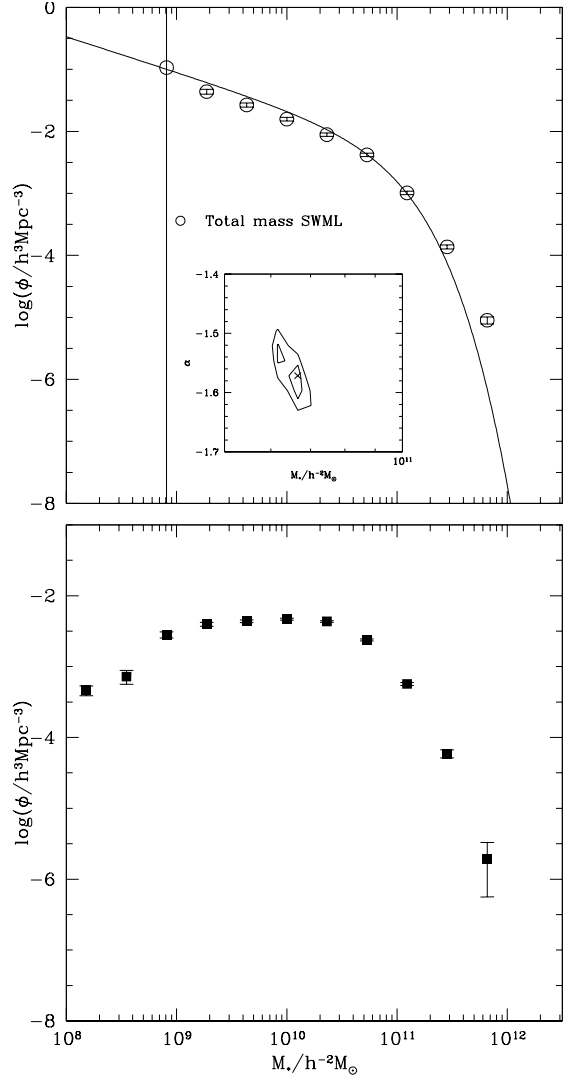


Figure 18. Stellar mass functions for galaxies as a whole and their disk and spheroid components (upper and lower panels) obtained using the SWML estimator. For the total mass function we also plot the Schechter function derived using the STY method (solid line), with the constraints on the parameters M_* and α shown in the inset. For the disk and spheroid mass functions, the dotted lines show the Schechter function which best fits the SWML data points.

the Υ (and K+E correction) of disk and spheroid components were estimated separately using measurements of the disk and spheroid colours. This would require performing spheroid-disk decompositions in multiple wavebands.

A quantity of interest is the ratio of stellar mass in disks to that in spheroids, averaged over the entire galaxy population. Integrating the stellar mass densities we obtain the average density of stars in disks and spheroids in units of the critical density. We find $\Omega_{\text{stars,disks}} = (0.486 \pm 0.004)h^{-1}10^{-3}$ and $\Omega_{\text{stars,spheroids}} = (0.465 \pm 0.006)h^{-1}10^{-3}$. These results are in good agreement with those of Benson et al. (2002) who found $\Omega_{\text{stars,disks}} = (0.51 \pm 0.08)h^{-1}10^{-3}$ and $\Omega_{\text{stars,spheroids}} = (0.39 \pm 0.06)h^{-1}10^{-3}$. We conclude that the fraction of stellar mass found in disks today is $51 \pm 1\%$.

If we adopt the same correction for the biased distribu-

Table 2. Best fitting Schechter function parameters for stellar mass functions of total, spheroid and disk components. For the total stellar mass function the best fit parameters are determined using the STY method. For the disk and spheroid stellar mass functions we instead fit a Schechter function to the non-parametric stellar mass function determined using the SWML method—these should be considered useful fitting functions only, not good fits in any statistical sense. For the SMBH mass function we find that a generalized Schechter function (see eqn. 4) provides a better fit to the data. The γ -parameter of this function is given in the final column.

Component	$\log_{10}(M_*/h^{-2}M_\odot)$	α	$\phi_0/h^3\text{Mpc}^{-3}$	γ
Total	10.82	-1.57	0.0035 ± 0.0002	1
Spheroid	10.87	-0.79	0.0019	1
Disk	10.64	-0.78	0.0035	1
SMBH	7.61	-0.65	0.0029	0.6

tion of $\cos i$ as we used in §4.3.1 we can construct stellar mass functions for disks and spheroids. The results are shown in Fig. 18, with parameters of Schechter function fits given in Table 2. After applying this correction we find stellar mass densities of $\Omega_{\text{stars,disks}} = (0.330 \pm 0.004)h^{-1}10^{-3}$ and $\Omega_{\text{stars,spheroids}} = (0.622 \pm 0.010)h^{-1}10^{-3}$ so that $(35 \pm 1)\%$ of stellar mass at $z = 0$ is found in disks.

As discussed above, a difficulty in converting from light to stellar mass is that we expect that disks and spheroids should have rather different mass-to-light ratios. In the above, we have used a mean mass-to-light ratio, estimated from our K+E method, to convert disk and spheroid light to disk and spheroid stellar mass. To examine the consequences of this, we perform the following simple experiment. We use our dataset to find the mean mass-to-light ratios as a function of redshift of systems identified as pure disks and pure spheroids (technically we identify systems which are at least 90% disk or 90% spheroid respectively). We then assume that in composite systems (i.e. galaxies with comparable fractions of light in their disk and spheroid) the mass-to-light ratios of the individual components are given by these mean values for pure systems. We can then estimate the stellar mass of the disks and spheroids using the total luminosity, measured S/T and the estimated mass-to-light ratios for disk stars and spheroid stars separately. We then compute stellar mass densities using these revised masses. We find that this changes our results by less than the errors quoted above. This approach represents only an approximate method for finding the mass-to-light ratios of individual components. Nevertheless, it suggests that such corrections will be small.

4.6 Black hole mass function

In the last few years, it has been conclusively demonstrated that many galaxies possess central supermassive black holes and that their mass is strongly correlated with the properties of the galaxy’s spheroid such as its luminosity, stellar mass and velocity dispersion (Kormendy & Richstone 1995; Magorrian et al. 1998; Merritt & Ferrarese 2001; Marconi & Hunt 2003; Häring & Rix 2004). Although there is only direct evidence for these black holes in bright galaxies, it seems quite plausible that galaxies of all sizes have a central black hole (e.g. Malbon et al. 2006).

From the mass function of galactic spheroids determined in §4.5, assuming that all spheroids contain a supermassive black hole at their centre, we can estimate the

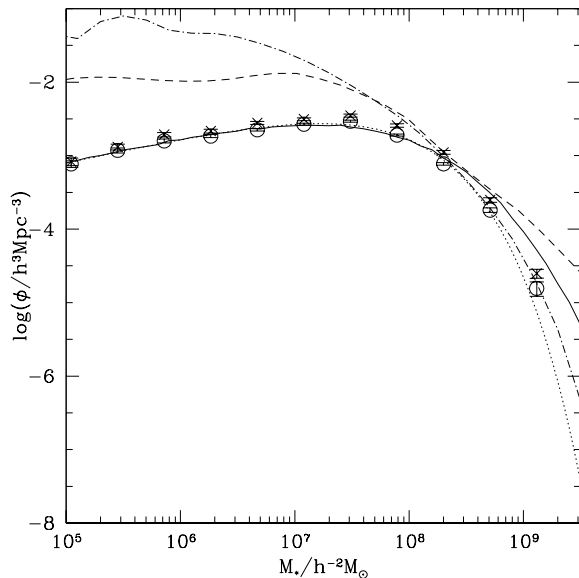


Figure 19. The mass function of supermassive black holes in galactic spheroids. Symbols show the black hole mass function implied by our observationally determined spheroid stellar mass function assuming that $M_\bullet/M_\odot = 1.6 \times 10^8 [M_{\text{spheroid}}/10^{11}M_\odot]^{1.12}$ (Häring & Rix 2004). The dotted line shows the Schechter function which best fits the SWML data points. Other lines show results from the galaxy formation model of Malbon et al. (2006) when using the parameters specified by Baugh et al. (2005; dot-dashed line) and Bower et al. (2006; dashed line).

mass function of supermassive black holes in the local Universe. We assume that the black hole mass is given by $M_\bullet/M_\odot = 1.6 \times 10^8 [M_{\text{spheroid}}/10^{11}M_\odot]^{1.12}$ (Häring & Rix 2004) and ignore any scatter in this relation since an accurate determination of the black hole mass function would first require a deconvolution of the (uncharacterized) error distribution of spheroid masses.

The resulting black hole mass function is shown in Fig. 19. Integrating this mass function gives a total black hole mass density in the local universe of $\rho_\bullet = (2.8 \pm 0.7) \times 10^5 h M_\odot \text{Mpc}^{-3}$ where we have included a scatter of 0.3 dex in the spheroid-SMBH mass relation (Häring & Rix 2004) and have included the error in the zero-point of the (Häring & Rix 2004) relation in our error budget. This result is

in agreement with previous determinations (Yu & Tremaine 2002; Aller & Richstone 2002; Marconi et al. 2004; McLure & Dunlop 2004; Shankar et al. 2004) based on much smaller samples of galaxies.

Applying our correction for the biased distribution of $\cos i$ results in an SMBH mass function shown by the crosses in Fig. 19. We find that a generalized Schechter function of the form

$$\phi(M_\bullet) = \phi_0 \left(\frac{M_\bullet}{M_*} \right)^\alpha \exp \left[- \left(\frac{M_\bullet}{M_*} \right)^\gamma \right] \quad (4)$$

provides a better fit to this SMBH mass function. Parameters of the generalized Schechter function which best fits the SWML data points are given in Table 2. The SMBH mass density after applying this correction is $\rho_\bullet = (3.77 \pm 0.97) \times 10^5 h M_\odot \text{Mpc}^{-3}$, which is consistent with previous determinations.

For comparison with our inferred black hole mass function, we show results from the recent model of Malbon et al. (2006) who incorporate a calculation of supermassive black hole growth into the GALFORM semi-analytic model of galaxy formation in a Λ CDM universe using methods similar to those first described by Kauffmann & Haehnelt (2000). The lines in Fig. 19 show their results for two different specific galaxy formation models. While the calculation based upon the parameters of Baugh et al. (2005) seems to match the abundance of the high-mass black holes quite well, neither model is able to reproduce the inferred low abundance of less massive black holes.

Before our results can be used to constrain such models strongly, it will be necessary to achieve a significantly better understanding of the uncertainties in the measured spheroid mass, and to perform the conversion from luminosity to stellar mass using a technique which accounts for the different stellar populations in the spheroid and disk.

4.7 The distribution of S/T

Finally, we examine the distributions of S/T obtained after applying the corrections for systematic effects described previously in this section. Not only are these distributions of interest in their own right, but they can also serve as valuable checks for additional systematic biases in our fitting procedure. We expect that the distribution of S/T (and therefore the mean S/T) should be independent of disk inclination and of redshift (at least for a sufficiently shallow sample that evolution can be ignored). In Fig. 20 we show the mean S/T (weighted by $1/V_{\text{max}}$) as a function of these two quantities, split by galaxy luminosity and redshift. The mean S/T seems to be reasonably independent of disk inclination, although there is some evidence for a rise at low $\cos(i)$. Note that we have excluded all galaxies for which we believe that the disk component of the photometric model has been used to fit some aspects of the true spheroid.

When we consider the mean S/T as a function of redshift we see a significant increase in S/T at low-redshifts for the fainter samples. Our sample is not sufficiently large to be unaffected by large-scale structure and, in fact, shows clear evidence of peaks in the redshift distribution presumably caused by large scale structure (see Fig. B5). This could create a redshift dependence in the mean S/T if, for example, a cluster of galaxies (likely to contain a substantial

population of elliptical galaxies) is present in the sample at low redshifts. Larger samples, unaffected by large scale structure, would be needed to address this issue further. For now, we simply note that for our brightest cut, the mean S/T seems quite independent of redshift.

Finally, we show in Fig. 21 the median S/T (and 10th and 90th percentiles) as a function of stellar mass. There is a strong trend for increasing S/T with stellar mass—the most massive galaxies are ellipticals. Interestingly, the median S/T is fairly constant at ~ 0.3 below around $3 \times 10^{10} h^2 M_\odot$, after which it rises rapidly to become close to unity. This is similar to the $3 \times 10^{10} M_\odot$ found by Kauffmann et al. (2003) to mark the division between galaxies with young stellar populations, low surface densities and low concentrations and those which are older, higher density and more concentrated.

5 SUMMARY AND CONCLUSIONS

We have used a sample of ~ 9000 galaxies extracted from the Sloan Digital Sky Survey to estimate the spheroid and disk luminosity and stellar mass functions in the local universe using the GALACTICA code of Benson et al. (2002). The 2D model fits to the surface brightness have revealed a bias in the recovered disk inclination angle arising from the lack of strong constraints on this parameter for most galaxies.

We find that at faint r-band luminosities, the light is dominated by disks whereas at bright luminosities, it is dominated by spheroids, with the changeover occurring at around the characteristic luminosity L_* . Integrating the luminosity functions, we find the total r-band luminosity densities in spheroids and disks to be $\rho_L = 0.611 \pm 0.008 \times 10^8 h L_\odot \text{Mpc}^{-3}$ and $\rho_L = 1.07 \pm 0.02 \times 10^8 h L_\odot \text{Mpc}^{-3}$ respectively. Thus, the disks contribute approximately two thirds of the total luminosity density. This is in contrast with the findings of previous studies (Schechter & Dressler 1987; Benson et al. 2002), based upon galaxy samples over 40 times smaller, which found the spheroid and disk luminosities to be very nearly equal.

Due to the fact that real galaxies do not always look like our idealized models we find a biased distribution of disk inclinations $\cos i$. This bias has been noted before by Simard et al. (2002), Tasca & White (2006) and Allen et al. (2006). The bias found here is identical to that found by Tasca & White (2006). Attempting to correct for this bias leads us to a conservative estimate for the disk contribution to the local luminosity density of between 43 to 64%. Applying the correction suggested by Tasca & White (2006) we find a disk contribution of $(53 \pm 3)\%$ in excellent agreement with their result of $(54 \pm 2)\%$.

Current *a priori* galaxy formation models are able to reproduce the disk and spheroid luminosity functions reasonably well—at least to the extent of predicting the correct trends of abundance with luminosity.

Using an approximate conversion of r-band light to stellar mass, we derive $\Omega_{\text{stars,disks}} = (0.486 \pm 0.004) h^{-1} 10^{-3}$ and $\Omega_{\text{stars,spheroids}} = (0.465 \pm 0.006) h^{-1} 10^{-3}$, in excellent agreement with the earlier work of Benson et al. (2002). Correcting for the bias in the $\cos i$ distribution leads to revised values of $\Omega_{\text{stars,disks}} = (0.458 \pm 0.005) h^{-1} 10^{-3}$ and $\Omega_{\text{stars,spheroids}} = (0.622 \pm 0.010) h^{-1} 10^{-3}$. Thus, stars in disks

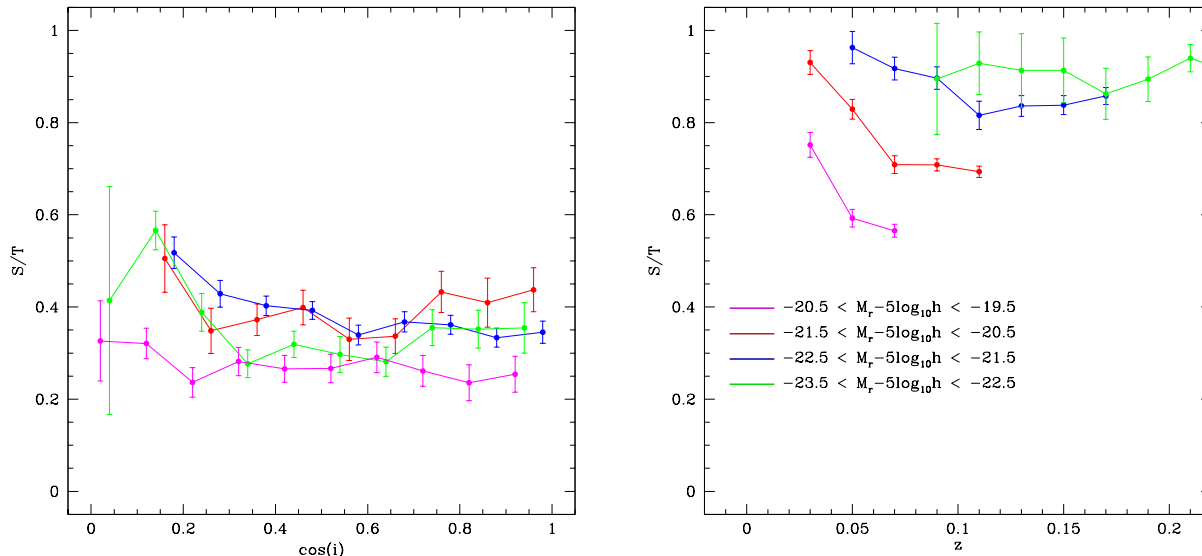


Figure 20. The mean, $1/V_{\max}$ weighted S/T ratio as a function of disk inclination (left-hand panel) and redshift (right-hand panel). Points show the mean S/T in each bin, while error bars show the 1σ error on the mean. In the left-hand panel, galaxies are split into four groups by luminosity and redshift at $M_r - 5\log_{10} h < -20.57$ and $z < 0.085$. The bright, low-redshift sample is shown by red points, the bright high-redshift sample by blue points, the faint low-redshift sample by magenta points and the faint high-redshift sample by green points. Galaxies for which the disk component of the model is thought to have been used to fit features of the observed spheroid have been excluded. In the right-hand panel galaxies are split by luminosity as indicated by the labels in the figure.

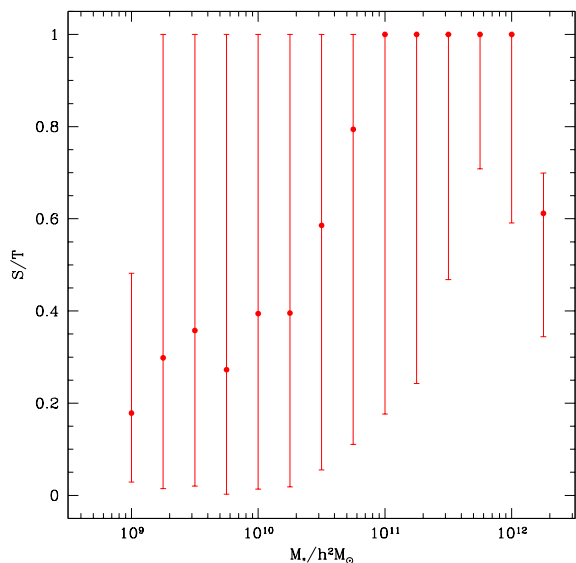


Figure 21. The distribution of S/T as a function of galaxy stellar mass. Galaxies are weighted by $1/V_{\max}$. Note that many galaxies are assigned S/T=1 during our process of correcting for cases where the disk in the photometric model has been fit to a true spheroid component. Red points with error bars show the median S/T as a function of stellar mass together with the 10th and 90th percentiles of the distribution.

contribute between 35 and 51% of the local stellar mass density. Bell et al. (2003) claim that between 50 and 75% of the stellar mass density comes from late-type galaxies. This range is in excellent agreement with our results. It should be

noted that the morphological selection chosen by Bell et al. (2003) would essentially select all galaxies with a spheroid-fraction of 0.5 or greater (and a large number of galaxies with smaller spheroid fractions) according to our calculations (see Fig. C2).

From the inferred spheroid mass function and the observed relation between central supermassive black hole mass and spheroid stellar mass, and assuming that all spheroids harbour a central black hole, we infer the supermassive black hole mass function. The associated black hole mass density in the local universe is $\rho_{\bullet} = (3.77 \pm 0.97) \times 10^5 h M_{\odot} \text{Mpc}^{-3}$, consistent with previous estimates. Improvements in the characterization of the errors in the spheroid mass function and in the stellar population modelling will enable a better estimate of the spheroid (and black hole) mass function.

We conclude that the local Universe contains around roughly comparable amounts of stars, by mass, in disks and in spheroids. This fundamental ratio is the outcome of the physical processes at play in the formation of the galaxy population.

ACKNOWLEDGMENTS

We are extremely grateful to Chris Miller for providing us with all of the SDSS EDR imaging data and Robert Nichol and Tomotsugu Goto for the encouragement given in the early days of this work. We also wish to thank Carlton Baugh for providing his code for computing K+E corrections, Rowena Malbon for providing theoretical predictions for black hole mass functions from the GALFORM semi-analytic model (www.galform.org) and Hans Walter Rix

and the anonymous referee for valuable discussions. We are particularly grateful to Simon White whose insightful comments on an early draft of the paper led us to revise our initial analysis and conclusions substantially. AJB acknowledges support from the Gordon & Betty Moore Foundation, and from a Royal Society University Research Fellowship during part of this work. CSF is the holder of a Royal Society Wolfson Research Merit award

Funding for the creation and distribution of the SDSS Archive has been provided by the Alfred P. Sloan Foundation, the Participating Institutions, the National Aeronautics and Space Administration, the National Science Foundation, the U.S. Department of Energy, the Japanese Monbukagakusho, and the Max Planck Society. The SDSS Web site is <http://www.sdss.org/>.

The SDSS is managed by the Astrophysical Research Consortium (ARC) for the Participating Institutions. The Participating Institutions are The University of Chicago, Fermilab, the Institute for Advanced Study, the Japan Participation Group, The Johns Hopkins University, Los Alamos National Laboratory, the Max-Planck-Institute for Astronomy (MPIA), the Max-Planck-Institute for Astrophysics (MPA), New Mexico State University, University of Pittsburgh, Princeton University, the United States Naval Observatory, and the University of Washington.

REFERENCES

- Abraham R.G., Valdes F., Yee H.K.C. & van den Bergh S., 1994, *ApJ*, 432, 75-90.
- Allen P. D., Driver S. P., Graham A. W., Cameron E., Liske J., de Propris R., 2006, *MNRAS*, 371, 2
- Aller M. C., Richstone D., 2002, *AJ*, 124, 3035
- Andredakis Y.C., Peletier R.F. & Balcells M., 1995, 275, 874A.
- Barnes J.E. & Hernquist L., 1992, *ARA&A*, 30, 705-742.
- Baugh C.M., Cole S. & Frenk C.S., 1996a, *MNRAS*, 282, L27-L32.
- Baugh C.M., Cole S. & Frenk C.S., 1996b, *MNRAS*, 283, 1361-1378.
- Baugh C. M., Lacey C. G., Frenk C. S., Granato G. L., Silva L., Bressan A., Benson A. J., Cole S., *MNRAS*, 356, 1191
- Balogh M., Eke V., Miller C., Lewis I., Bower R.G., Couch W., Nichol R., Bland-Hawthorn J., Baldry I.K., Baugh C., Bridges T., Cannon R., Cole S., Colless M., Collins C., Cross N., and Dalton G., de Propris R., Driver S.P., Efstathiou G., Ellis R.S., Frenk C.S., Glazebrook K., Gomez P., Gray A., Hawkins E., Jackson C., Lahav O., Lumsden S., Maddox S., Madgwick D., Norberg P., Peacock J.A., Percival W., Peterson B.A., Sutherland W. & Taylor K., 2004, *MNRAS*, 348, 1355-1372.
- Balogh, M. L., Bower, R. G., Smail, I., Ziegler, B. L., Davies, R. L., Gaztelu, A., & Fritz A., 2002, *MNRAS*, 337, 256B.
- Balogh M.L., Baldry I.K., Nichol R., Miller C., Bower R. & Glazebrook K., 2004, *ApJ*, 615, 101
- Beijersbergen M., de Blok W.J.G. & van der Hulst J.M., 1999, 351, 903-919.
- Bell E. F., McIntosh D. H., Katz N., Weinberg M. D., 2003, *ApJS*, 149, 289
- Benson A. J., Frenk C. S., Sharples R. M., 2002, *ApJ*, 574, 104B.
- Benson A. J., Lacey C. G., Frenk C. S., Baugh C. M., Cole S., 2004, *MNRAS*, 351, 1215
- Bernstein G. M., Jarvis M., 2002, *AJ*, 123, 583
- Blanton M. R. et al., 2003, *ApJ*, 592, 819
- Bower R. G., Benson A. J., Malbon R., Helly J. C., Frenk C. S., Baugh C. M., Cole S., Lacey C. G., 2006, *MNRAS*, 370, 645
- Bertin E. & Arnouts S., 1996, *A&A*, 117, 393.
- Bruzual A. G., & Charlot S., 1993, *ApJ*, 405, 538B.
- de Jong R. S., 1996, *A&AS*, 118, 557-573.
- de Vaucouleurs G., 1961, *ApJS*, 5, 233.
- Dressler A., 1980, *ApJ*, 236, 351-365.
- Efstathiou G., 1993, *Les Houches Lectures: Observations of Large-Scale Structure in the Universe*, Elsevier Science Publishers.
- Efstathiou G., Ellis R. S. & Peterson B. A., 1988, *MNRAS*, 232, 431.
- Eggen O.J., Lynden-Bell D. & Sandage A.R., 1962, *ApJ*, 136, 748.
- Fall S. M., 1979, *Nature*, 281, 200
- Fall S. M., Efstathiou G., 1980, *MNRAS*, 193, 189
- Felten J.E., 1977, *AJ*, 82, 861-878.
- Fukugita M., Shimasaku K. & Ichikawa T., 1995, *PASP*, 107, 945.
- Gadotti D., Kauffmann G., "Multi-Band Bar/Bulge/Disk Image Decomposition of a Thousand Galaxies", in "Stellar Populations as Building Blocks of Galaxies", proceedings of the IAU Symp. 241, La Palma, Spain, December 2006, A. Vazdekis, R. Peletier (eds.)
- Gardner J.P., Sharples R.M., Carrasco B.E. & Frenk C.S., 1996, *MNRAS*, 282.
- Goto T., Okamura S., McKay T.A., Bahcall N.A., Annis J., Bernardi M., Brinkmann J., Gómez P.L., Hansen S., Kim R.S.J., Sekiguchi M. & Sheth R.K., 2002, *PASJ*, 54, 515-525.
- Griffiths R.E., Casertano S., Ratnatunga K.U., Neuschaefer L.W., Ellis R.S., Gilmore G.F., Glazebrook K., Santiago B., Huchra J.P., Windhorst R.A., Pascarelle S.M., Green R.F., Illingworth G.D., Koo D.C. & Tyson A.J., 1994, *ApJL*, 435, L19-L22.
- Häring N., Rix H.-W., 2004, *ApJ*, 604, 89
- Hatton S., Devriendt J. E. G., Ninin S., Bouchet F. R., Guiderdoni B., Vibert D., 2003, *MNRAS*, 343, 75
- Kauffmann G., White S. D. M., Guiderdoni, B. 1993, *MNRAS*, 264, 201
- Kauffmann G., Charlot S., White S. D. M. 1996, *MNRAS*, 283, 117
- Kauffmann G., Charlot S., 1998, *MNRAS*, 297, 23
- Kauffmann G., Haehnelt M., 2000, *MNRAS*, 358, 2121
- Kauffmann G. et al., 2003, *MNRAS*, 341, 54
- Kent, S. M., 1985, *AJSS*, 59, 115-159.
- Kormendy J., Richstone D., 1995, *ARA&A*, 33, 581
- Krist J., 1995, *ASP Conf. Ser. 77: Astronomical Data Analysis Software and Systems IV*, 349.
- Lambas D. G., Maddox S., Loveday J., 1992, *MNRAS*, 258, 404
- Lupton R.H., Gunn J.E., Ivezić Z., Knapp G.R., Kent S. & Yasuda N., 2001, *ADASS*, 10, 269L
- Magorrian J., et al., 1998, *AJ*, 115, 2285
- Marconi A., Hunt L. K., 2003, *ApJ*, 589, L21
- Marconi A., Risalti G., Gilli R., Hunt L. K., Maiolino R., Salvati M., 2004, *MNRAS*, 351, 169
- Malbon R., Baugh C. M., Frenk C. S., Lacey C. G., 2006, *MNRAS* submitted (astro-ph/0607424)
- McLure R. J., Dunlop J. S., 2004, *MNRAS*, 353, 1390
- Merritt D., Ferrarese L., 2001, *MNRAS*, 320, L30
- Metropolis N., Rosenbluth A., Rosenbluth M., Teller A. & Teller E., 1953, *Journal of Chemical Physics*, 21, 1087
- Mo H. J., Mao S., White S. D. M., 1998, *MNRAS*, 295, 319
- Moffat A.F.J., 1969, *AAP*, 3, 455
- Nakamura O., Fukugita M., Yasuda N., Loveday J., Brinkmann J., Schneider D.P., Shimasaku K. & SubbaRao M., 2003, *AJ*, 125, 1682-1688.
- Nelson A. E., Simard L., Zaritsky D., Dalcanton J. J. & Gonzalez A. H., 2002, *AJ*, 567, 144.
- Press W.H., Teukolsky S.A., Vetterling W.T. & Flannery B.P., 1992, *Numerical Recipes in FORTRAN*, Cambridge University Press, Chapter 10.
- Ratnatunga K.U., Griffiths R.E. & Ostrander E.J., 1999, *AJ*, 118, 86-107.

- Salpeter E.E., 1955, ApJ, 121, 161
 Sandage A., Tammann G.A. & Yahil A., 1979, ApJ, 232, 352-364.
 Schechter P., 1976, ApJ, 203, 297-306.
 Schechter P.L. & Dressler A., 1987, AJ, 94, 563S.
 Sérsic J.-L., 1968, *Atlas de Galaxias Australes*, Cordoba: Obs. Astronomico, Generalised $R^{1/4}$ law
 Shankar F., Salucci P., Granato G. L., De Zotti G., Danese L., 2004, MNRAS, 354, 1020
 Shimasaku K., Fukugita M., Doi M., Hamabe M., Ichikawa T., Okamura S., Sekiguchi M., Yasuda N., Brinkmann J., Csabai I., Ichikawa S., Ivezić Z., Kunszt P.Z., Schneider D.P., Szokoly G.P., Watanabe M. & York D.G., 2001, AJ, 122, 1238-1250
 Simard L., Willmer C.N.A., Vogt N.P., Sarajedini V.L., Phillips A.C., Weiner B.J., Koo D.C., Im M., Illingworth G.K. & Faber S.M., 2002, ApJS, 142, 1
 Somerville R. S., Primack J. R., 1999, MNRAS, 310, 1087
 Stoughton C., et al., 2002, AJ, 123, 485S
 Strateva I., et al., 2001, AJ, 122, 1861
 Tasca L., White S. D. M., 2005, in “Multiwavelength mapping of galaxy formation and evolution”, Proceedings of the ESO Workshop, eds. A. Renzini and R. Bender., Springer, Berlin, p.465
 Tasca L., White S. D. M., 2006, astro-ph/0507249
 Trujillo I., Aguerri J.A.L., Cepa J. & Gutiérrez C.M., 2001, MNRAS, 328, 977-985
 Wadadekar Y., Robbason B. & Kembhavi A., 1999, AJ, 117, 1219-1228
 Yu Q., Tremaine S., 2002, MNRAS, 335, 965

APPENDIX A: METHODS FOR QUANTITATIVE GALAXY MORPHOLOGY

In this Appendix, two independent methods for spheroid-to-disk decompositions of galaxies are described and compared. A number of tests are performed to reveal and estimate any potential biases in the decomposition codes.

A1 Introduction to spheroid-to-disk decomposition

To first approximation, the surface brightness of a galaxy can be expressed as the sum of a highly concentrated central component, the spheroid, and an extended disk. Empirically, the surface brightness profiles of spheroids and disks are well represented by the following functions,

$$I_s = I_e \exp(-7.67[(r/r_e)^{1/4} - 1]), \quad (\text{A1})$$

an $r^{1/4}$ -law, for the spheroid (de Vaucouleurs 1961), where r_e is the half-light radius and I_e is the surface brightness at r_e , and,

$$I_d = I_0 \exp(-r/r_d), \quad (\text{A2})$$

an exponential-law for a face-on disk, where r_d is the exponential disk scale-length and I_0 is the central intensity.

Equations A1 and A2 can be used to construct model images of the galaxy. Comparison with the surface brightness distribution of each galaxy, including the effects of inclination, enables the fitting parameters to be determined.

Andredakis et al. (1995) used this technique to fit the spheroid components of a sample of morphologically selected galaxies with types ranging from S0 to Sbc. They assumed a more general type of profile,

$$I_s = I_e \exp(-b_n[(r/r_e)^{1/n} - 1]), \quad (\text{A3})$$

first proposed by Sérsic (1968), where n is often referred to as the Sérsic index and determines the ‘peakiness’ of the profile and b_n is a constant dependent on the value of n . Andredakis et al. found that the value of n varied systematically from 1 for late-type spheroids to 6 for early-type spheroids. de Jong (1996) also suggested that the spheroids of field spirals are better fit using a pure exponential (i.e. $n = 1$) profile.

A2 Methods for 2-dimensional spheroid-to-disk decomposition

A2.1 Fitting parameters revisited

On a Cartesian grid (x, y) the effective r in eqns. (A1) and (A2) become

$$r^2(x, y) = \frac{1}{e_s} [x \cos(\theta_s) - y \sin(\theta_s)]^2 + e_s [x \sin(\theta_s) + y \cos(\theta_s)]^2 \quad (\text{A4})$$

$$(\text{A5})$$

and

$$r^2(x, y) = [x \cos(\theta_d) - y \sin(\theta_d)]^2 + \frac{1}{\cos^2(i)} [x \sin(\theta_d) + y \cos(\theta_d)]^2 \quad (\text{A6})$$

respectively. Here θ_s and θ_d are the spheroid and disk position angles, where a position angle is defined as the angle of orientation of the galaxy’s main axis with respect to some coordinate system, and e_s is the spheroid ellipticity used to describe the deviation from circularity of the spheroid component

In terms of a $r^{1/n}$ spheroid and an exponential disk, and including the sky background, 2D decomposition usually requires a total of 13 free parameters:

- total flux in the galaxy;
- S/T: ratio of the amount of light in the spheroid to the total amount of light;
- r_e : effective radius of the spheroid;
- e_s : spheroid ellipticity;
- θ_s : spheroid position angle;
- r_d : scale length of the disk;
- i : inclination angle of the disk;
- θ_d : disk position angle;
- x_c, y_c : subpixel offset of the galaxy centre;
- residual sky background level;
- FWHM of the point spread function (PSF);
- n : Sérsic index.

In order to make the decomposition procedure as accurate and fast as possible, the following points must be taken into account:

- The PSF smooths the galaxy image and so to achieve accurate fits, it must be modelled accurately and included in the mock images.
- The fit is carried out using small “thumbnail” regions around each galaxy. The size of the thumbnail must be small enough to enable a fast fit to the image, but large enough to include all regions of the galaxy with significant signal-to-noise.

- The mean sky background level should be ~ 0 since the decomposition codes are designed to work with no (or very little) background; any excess sky light can be mistaken for galaxy light and lead to incorrect parameter estimation.

We now explore the similarities and differences of two independent multi-dimensional fitting codes, the GIM2D code of Simard et al. (2002) and the GALACTICA code of Benson et al. (2002).

A2.2 Galaxy image 2D decomposition (Gim2D)

GIM2D is a publicly available code written by Simard et al. (2002) and widely used for automated spheroid-to-disk decompositions of galaxy light profiles (Balogh et al. 2002; Nelson et al. 2002). This code was purposely written for imaging with the Hubble Space Telescope Wide Field and Planetary Camera which has a very well modelled PSF (Krist 1995). The code can also be used for ground-based imaging data but, in this case, special attention must be given to the much larger and less well defined PSF.

Object Detection

To extract a postage-stamp image around each galaxy, GIM2D relies upon SExtractor (Bertin & Arnouts 1996). SExtractor determines the galaxy centroid position and the area at the faintest detected isophote to be obtained and also measures the mean level of the sky background for each galaxy (a 3σ threshold is usually sufficient to discriminate between the object and the background). GIM2D extracts a postage-stamp of size equal to a multiple of a galaxy isophotal area. A value of $15 \times \text{iso_area}$ was found to be optimum. The sky-background is not recommended to be treated as a free fitting parameter in GIM2D because the underlying sky is not well known and can potentially bias the output (Simard et al. 2002). However, before the decomposition procedure is initiated, GIM2D uses the pixels flagged by SExtractor as belonging to the background (flag value 0) to recompute the background value, therefore ensuring that the mean sky level is close to zero. All the background pixels and also pixels flagged as ‘bad’ (flag value -2) by SExtractor are subsequently excluded from the fitting altogether.

Point Spread Function

During the minimization in GIM2D, the PSF is kept fixed. For ground-based imaging, the PSF is obtained from a bright unsaturated stellar image; for HST data, an analytic PSF modelled using the Tiny Tim software is used (Krist 1995).

Minimization Technique: Metropolis Algorithm

GIM2D allows up to 12 parameters to be fit⁵ and uses the Metropolis algorithm (Metropolis et al. 1953) to search for the minimum χ^2 in this multi-dimensional parameter space. Before starting the Metropolis algorithm, GIM2D works in the Initial Condition Filter (ICF) mode, i.e. it creates a user-specified number of models between the limits of the user-specified multi-dimensional parameter

space. The ICF computes the model likelihoods and sets the sampling origin to the parameters of the best model, making it a subvolume to be exploited by the Metropolis Algorithm.

GIM2D Outputs

After finding the model that corresponds to the highest likelihood, GIM2D produces a residual (object - model) map and calculates the value of the corresponding χ^2_ν . If $\chi^2_\nu \sim 1$ and the residual map has no remaining galaxy structure, the best-fit model is accepted.

A2.3 GALACTICA

Introduction

The 2-dimensional decomposition code described here is based on a technique proposed by Wadadekar et al. (1999). GALACTICA was developed by Benson et al. (2002) and assumes the standard empirical formalisms for the 2-dimensional surface brightnesses of a galaxy spheroid and disk components respectively (eqns. A1 & A2).

Object detection

To locate and extract a postage-stamp image around every galaxy, GALACTICA employs the same method as GIM2D. SExtractor is also used to measure the mean level of the sky background for each galaxy (a 3σ threshold is usually sufficient to discriminate between the object and the background) and this value is subtracted from the corresponding galaxy image. To mask any overlapping objects within the extracted postage-stamp GALACTICA relies upon an in-built masking algorithm which finds any objects that contaminate the galaxy of interest and masks them out. The galaxy itself is also detected by the algorithm using a 5σ threshold above the sky background. Pixels which have not been flagged as belonging to any of the detected objects are used in the sky background fitting.

Point spread function: Moffat profile

To correct for the effect of seeing, the GALACTICA code generates a Moffat profile star image (Moffat 1969) of a given full-width half-maximum (FWHM) expressed in terms of $\sigma_{\text{PSF}} = \text{PSF}_{\text{FWHM}}/2.35$. This analytic profile is defined by

$$\text{PSF}(r) = \text{const}/[1 + (r/\alpha)^2]^\beta \quad (\text{A7})$$

and is thought to represent the overall PSF shape better than a pure Gaussian which only approximates the core regions. Here α represents the width of the PSF and is related to the $\text{FWHM} = 2\alpha\sqrt{2^{1/\beta} - 1}$ (Trujillo et al. 2001). β governs how ‘peaky’ the PSF profile is (the larger β is, the more Gaussian-like the profile becomes). A value of $\beta = 4.5$ is used throughout. The α parameter can be fine-tuned to a particular dataset using the average FWHM for the data. GALACTICA lets σ_{PSF} be a free fitting parameter to allow for any small changes in the PSF between the position of the stars in the image and the galaxy position.

Minimization technique: Powell’s method

The code requires explicit initialization of the fitting parameters. The initial value of the S/T ratio is always fixed at 0.5, although starting with a value of S/T randomly distributed in the range 0 to 1 has no effect on the recovered S/T distribution. The starting position angles of the disk

⁵ Sersic index is held fixed at 4.

and spheroid components, their characteristic radii and the disk inclination angle are calculated directly from the image. The ranges over which parameters are allowed to vary during the fitting are specified and fitting outside these limits is not possible.

χ^2 is minimized in a 12-parameter space; the Sérsic index is set to $n = 4$ and the FWHM of the PSF and the residual sky background level are additional fitting parameters not included in GIM2D. Note that in fitting the total flux in the galaxy GALACTICA we find a typical variation of only 5% around the value estimated from SDSS photometry. The minimization routine is also rather different from the one used by GIM2D. In GIM2D every parameter is varied at each step according to the ‘temperature’ of the fit. In GALACTICA one parameter is minimized at a time, i.e. all but one parameters are ‘frozen’ until a minimum for this parameter is found and the process is repeated for the entire set of parameters until the global minimum is found —the essence of Powell’s method (see Press et al. 1992 for further details). This method is good for finding a global extremum but is typically slower than the Metropolis algorithm employed by GIM2D.

GALACTICA outputs and error estimation

After convergence is achieved, the best-fit parameters are output along with the best-fit model image and the residual map obtained by subtracting the model galaxy from the real image. The value of χ^2 per degree of freedom, χ^2_ν , is then calculated. Errors on the fitted parameters are obtained using a Monte Carlo method: we create 30 realizations of the best fitting model for each galaxy by adding random noise, drawn from a Poisson distribution, to the model image. The distribution of the best-fitting parameters of the model realizations is then used to estimate the uncertainty in the fit. This method allows the uncertainties in the image parameters to be obtained without any assumptions about their distribution.

A3 GIM2D vs. GALACTICA comparison

A3.1 Introduction

The previous section described two independent codes for estimating basic galaxy structural parameters. Although these codes assume the same analytic surface brightness profiles to fit the spheroid and disk components, the differences in the number of fitting parameters and in the minimization techniques are sufficiently large to make a comparison interesting and important.

We first note the following points relevant to the comparison:

- both codes assume a fixed value of $n = 4$;
- the sky background is always kept fixed by GIM2D although the code is allowed to recompute and correct the background level before the minimization procedure starts;
- GALACTICA always treats the sky background as a free parameter;
- the ellipticity is defined differently: GIM2D fits $e = 1 - b/a$ while GALACTICA fits a/b ;

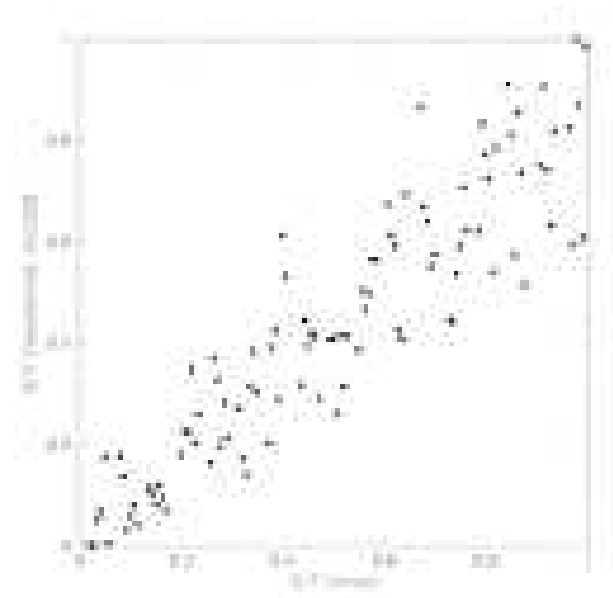


Figure A1. Correlation between the input S/T ratios for 100 model galaxies and the best-fit S/T ratios recovered using GIM2D. The scatter around the mean is $\sigma_{\text{rms}} = 0.10$. Note a small systematic underestimate of S/T, accompanied by increased scatter, for large input values. The recovered characteristic radii of these galaxies are the largest and the sky background recalculated by GIM2D for these galaxies is high. The resulting confusion between the background and an extended surface brightness profile accounts for this effect.

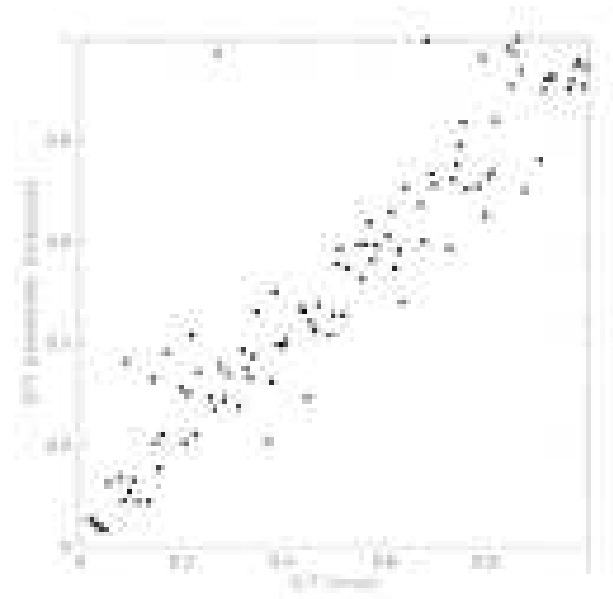


Figure A2. Correlation between the input S/T ratios for 100 model galaxies and the best-fit S/T ratios recovered using GALACTICA. The scatter around the mean is $\sigma_{\text{rms}} = 0.11$.

Table A1. Parameter ranges used for constructing mock galaxies.

Parameter	Low limit	High limit
S/T	0.0	1.0
$r_{e,d}$ (pixels)	1	12
e_s	0.0	0.8
i (degrees)	0.0	90.0
$\theta_{s,d}$ (degrees)	0.0	180.0
FWHM (")	1.4	1.4

- the seeing is fixed in GIM2D but in GALACTICA it is allowed to fluctuate between $\pm 5\%$ of the specified σ_{PSF} ;

- the position angles in GIM2D are defined with respect to the y -axis of a Cartesian system while in GALACTICA they are defined clockwise from the x -axis. (The position angles of the spheroid and disk are allowed to vary in both codes; a large difference between these can be a signature of a barred structure; Simard et al. 2002).

To quantify the performance of the codes, a series of tests were conducted as we now describe.

A3.2 Tests using model galaxies

A useful in-built feature of both GALACTICA and GIM2D is the ability to create model galaxies. The initial tests and code comparisons described below were carried out on model galaxies generated “internally” by GALACTICA.

Model galaxies were constructed adopting parameter values chosen at random between realistic limits (Table A1) and matching the total counts measured in a typical real galaxy. Poisson noise was added to the model galaxy after its image was convolved with an analytic Moffat PSF corresponding to a typical value of the seeing. This PSF is subsequently used as the GIM2D PSF. Model galaxies were analyzed with both codes using exactly the same procedures as for real galaxies.

Comparison of the known input S/T values and the values output by GIM2D and GALACTICA for 100 model galaxies are shown in Figs. A1 and A2 respectively. In both cases the codes recover the input S/T very well. The scatter in the recovered S/T ratios is $\sigma_{\text{rms}} \sim 0.10$. The remaining parameter recoveries are shown in Figs. A3 and A4.

The results shown in Figs. A1 to A4 demonstrate that both GIM2D and GALACTICA produce, on the whole, reliable spheroid/disk decompositions for a set of artificial galaxies generated according to the model assumed by the code. A more stringent test of the codes is to apply them to model galaxies generated independently of the codes themselves. Model galaxies were therefore externally created using the IRAF task MKOBJ.

The model parameters were taken from Table A1; a model galaxy is created for given values of the size, orientation and ellipticity (in this case defined as b/a) and the image is convolved with a specified seeing. A useful feature of this approach is that a real science frame can be fed into MKOBJ and the model galaxy added to a blank patch of the sky on this science frame. By matching, on average, the counts in a real galaxy, this procedure ensures that the artificial image has similar noise characteristics to the real data.

To generate the model galaxies several SDSS r' -band frames were extracted, each typically containing ~ 5 SDSS catalogued galaxies. Each frame was taken from a different patch of the sky. Counts associated with the SDSS galaxies were measured using the SExtractor `flux_best` parameter. In order to test the decomposition algorithm over a realistic range of galaxy properties, this procedure was applied to galaxies spanning a range of apparent magnitude and apparent shape and size. The model galaxies were inserted across the blank regions of the sky in the original frames. The postage-stamps for these galaxies were extracted using SExtractor and the decomposition codes run treating the extracted model galaxies just as the real ones.

The results of the GIM2D decompositions of the model galaxies are shown in Fig A5. The agreement between the input and output S/T ratios for the pure exponential disks (S/T= 0) is excellent. However, the recovered S/T ratio for S/T= 0.5 is biased by $\Delta\text{S/T}= 0.1$ and for S/T= 1.0 it is biased by $\Delta\text{S/T}= 0.2$. The tendency is always to underestimate the amount of spheroid or, equivalently, overestimate the amount of disk. GIM2D can be fine-tuned to recover the input S/T ratios with $\Delta\text{S/T} \simeq 0.1$ across the full S/T range. For this, GIM2D requires that the size of the zone around the lowest SExtractor isophote used in the re-calibration of the sky background should be set to ~ 30 pixels (the default value is 10 pixels). This ensures that any faint galaxy flux does not contribute to the re-calibrated background flux thus minimizing any bias in S/T.

The results of the GALACTICA decompositions of the model galaxies are shown in Fig. A6. For the pure exponential disks the recovered S/T ratios are, again, very good. As before, for larger S/T, this ratio is underestimated and peaks at S/T= 1.0, implying that many pure $r^{1/4}$ galaxies have acquired a fictitious disk component. There appears to be no correlation between the size of the underestimation and the magnitude or scale radius of the input galaxy but a weak correlation with the minor/major axis ratios: the S/T deviation is largest for the most elliptical profiles. The most prominent correlation, however, is between the recovered S/T ratio and the sky background. As discussed earlier, the GALACTICA code allows the sky background to fluctuate a little to allow for uncertainties in the estimated background. The fact that the deviation between the input and the output S/T ratios is largest when the ‘fitted’ background is smallest implies that an extraneous disk component is found where, in fact, the extra counts are due to the sky background. Since there is no sharp cut-off in either the spheroid or the disk, at the galaxy edges the galaxy surface brightness profile and the sky background are indistinguishable.

GIM2D performs marginally better than GALACTICA in the recovery of the S/T ratios. However, both codes show similar biases in the decompositions. This is despite the fact that we allow the background and PSF to be fit by GALACTICA but not by GIM2D indicating that this choice does not significantly bias our results. The relative performance of these two codes on a set of real galaxies is compared next. This allows a more realistic comparison of the codes but, of course, there is no *a priori* correct answer.

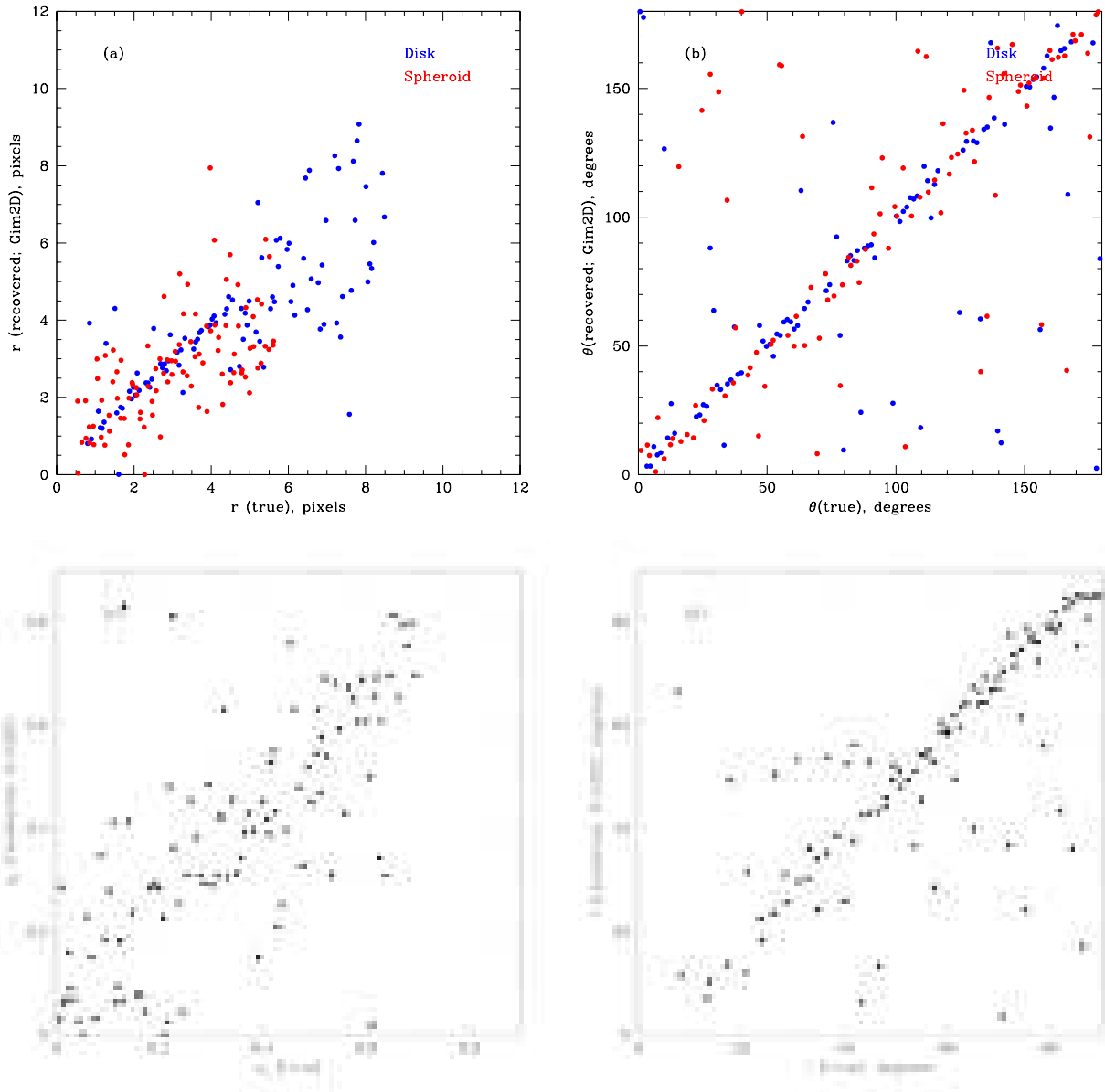


Figure A3. Correlations between input and recovered values of the characteristic radius, position angle, ellipticity and inclination for 100 model galaxies created using the GALACTICA code and decomposed using GIM2D. a) Disk and spheroid radii. b) Disk and spheroid position angles. c) Spheroid ellipticity. d) Disk inclination. There is a saturation at $i = 85^\circ$ which is the upper limit that GIM2D allows for the disk inclination. All other parameters correlate well although significant scatter is seen.

A3.3 Tests using real galaxies

To ensure a uniform sampling of the [S/T, apparent magnitude] space, the comparison was carried out using a subsample of SDSS galaxies selected in bins of 0.5 in apparent magnitude and 0.2 in S/T ratio (as determined by GALACTICA). Unsaturated stellar images with high S/N were extracted from the SDSS galaxy frames and used in the GIM2D PSF deconvolution. The GALACTICA Moffat PSF was fine-tuned to fit the SDSS data well. Fig. A7 demonstrates a significant correlation (Spearman rank correlation coefficient of 0.74) between the S/T ratios for ~ 350 SDSS galaxies inferred using GIM2D and GALACTICA. There are no systematic differences between

the results of the two codes. The correlations between other parameters are displayed in Fig. A8.

APPENDIX B: GALACTICA METHODOLOGY

B1 Code speed limitations and galaxy binning

The SDSS galaxy sample contains less than 200 galaxies whose postage-stamp size exceeds 91 pixels on a side. To reduce the processing time, these large postage-stamps were binned 2×2 . This has the added advantage that large nearby bright galaxies are sampled at a resolution comparable to

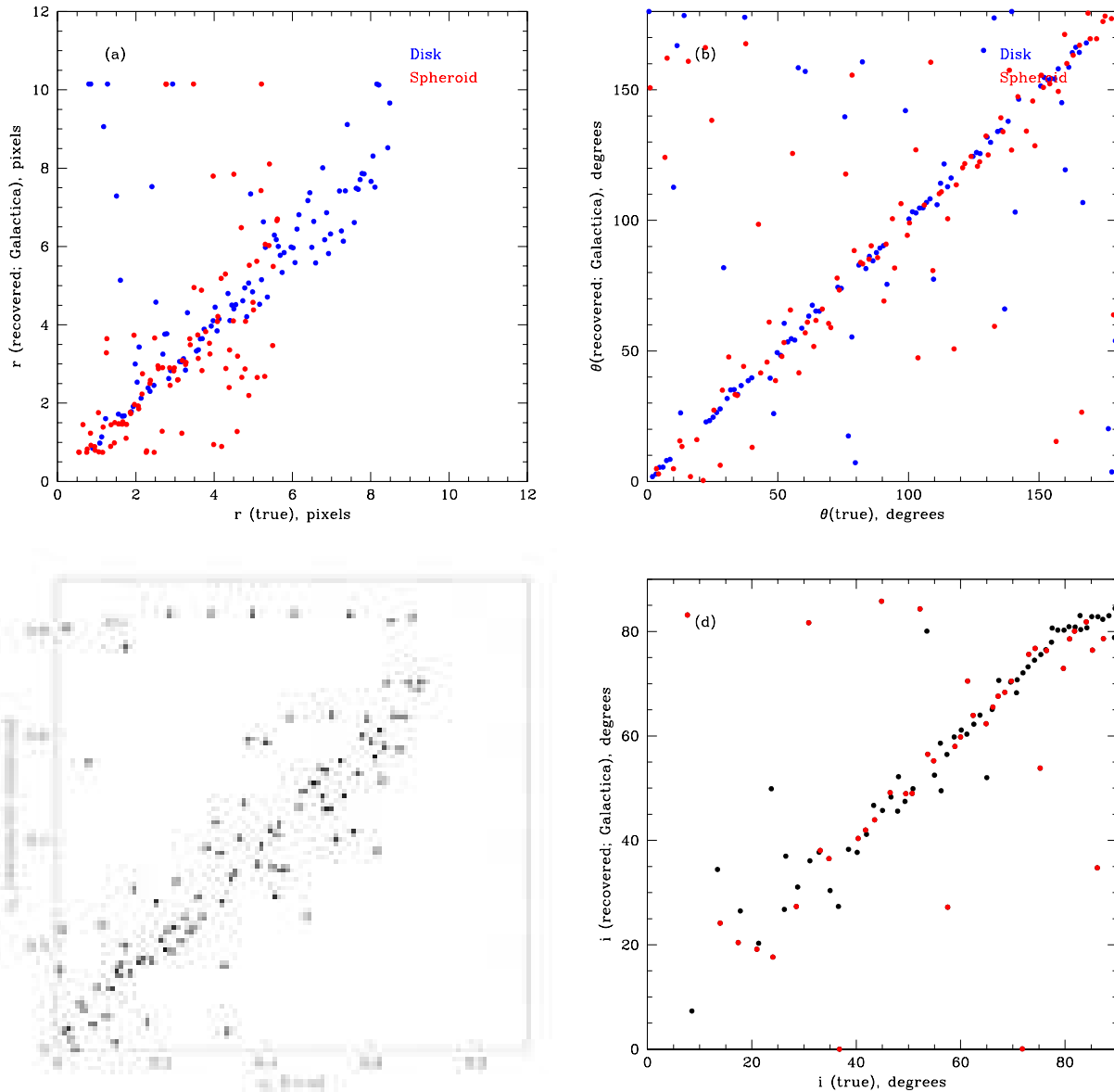


Figure A4. Correlations between input and recovered values of the characteristic radius, position angle, ellipticity and inclination for 100 model galaxies created and decomposed using the GALACTICA code. a) Disk and spheroid radii. Note that the reconstruction seems to hit the upper limit on the characteristic radii when the input radii are very small or very large. b) Disk and spheroid position angles. c) Spheroid ellipticity. Note that a number of very elliptical spheroids are found. These are mostly galaxies which have very small spheroids. d) Disk inclination. Note an apparent saturation at $i \sim 85^\circ$. Even though the GALACTICA code allows the disk to be fully inclined ($i = 90^\circ$), the reconstruction avoids this upper limit.

that of more distant objects. To make sure that the binning procedure does not bias the recovery of the galaxy S/T ratios, we carried out a series of tests.

Several model galaxies were created using our standard procedure (see Appendix A3.2) and binned using the IRAF task BLKAVG. GALACTICA was then used to perform the fitting ensuring that the pixel for the binned image is set to $2 \times$ the normal pixel size ($2 \times 0.396''$) and that the noise properties in this ‘super-pixel’ are changed accordingly. Figs. B1 and B2 show fits to model galaxies consisting either of a pure exponential disk or a pure $r^{1/4}$ spheroid after the original

model images were binned by 2×2 . In the case of the pure exponential disk, the fit to the model is perfect. The fit to the pure $r^{1/4}$ galaxy, however, shows a similar bias to that seen for the unbinned data (Appendix A), as indicated by the low value of the recovered S/T = 0.8. This shows that the binning in itself is not responsible for the observed S/T bias. The 2×2 binning was therefore applied to all the SDSS galaxies whose postage-stamps are greater than 91×91 pixels.

The binning works very well if the binned galaxy does not exhibit much internal structure (as in the model galax-

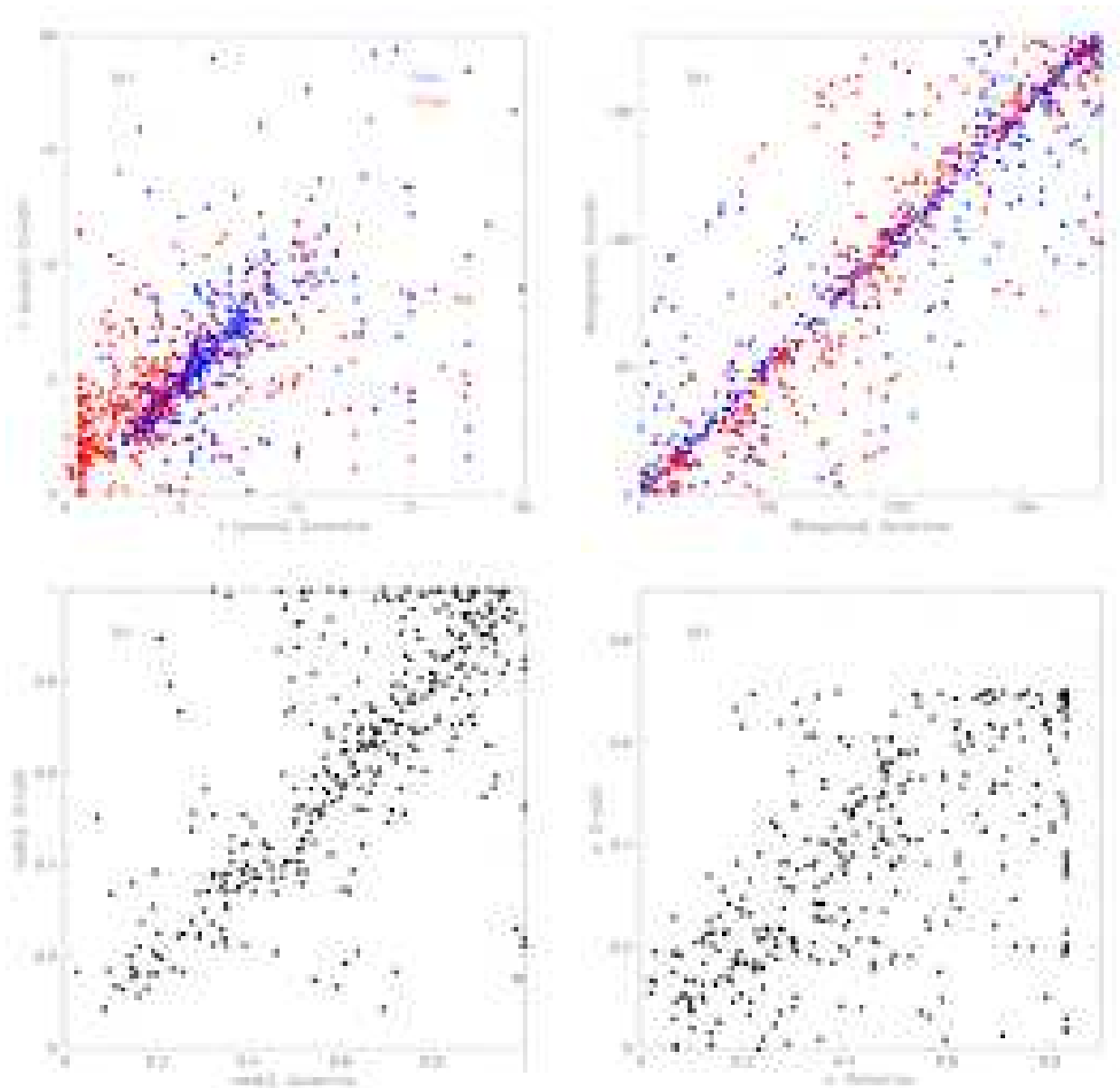


Figure A8. Correlation between various parameters inferred using GIM2D and GALACTICA for a sample of 350 SDSS galaxies. No systematic differences in the recovered parameters are apparent although the scatter can be quite large.

ies). However, for a galaxy which exhibits significant internal structure, a fit with $\chi^2_\nu > 2.0$ is more typical. Whether decomposing such galaxies even without binning would lead to a good fit is unclear as demonstrated for 2 SDSS galaxies in Fig. B3 and B4. The top images in both figures show the postage stamp and the residual map for the unbinned galaxy which has size 101×101 pixels. (To speed up the calculation, the postage stamp was trimmed by 5 pixels on either side.) The bottom panels show the corresponding images for the binned versions of the same galaxy.

The galaxy in Fig. B3 exhibits much more internal structure than the galaxy in Fig. B4, as is clear from both the value of χ^2_ν and the residual image. This supports the conclusion that galaxies which exhibit internal structure are poorly fit irrespective of whether they are binned or not.

The recovered S/T ratios for the unbinned and binned data, although different, are consistent with the typical errors in the S/T ratio. We conclude that the S/T distribution of the final SDSS galaxy sample is not biased by binning these large, bright nearby objects (most of which contribute to the faint-end of the luminosity function – see Section 4).

B2 SDSS data and the goodness-of-fit

The selected SDSS sample of 8839 galaxies is too large for each of the residual images to be inspected by eye to ensure a satisfactory decomposition as suggested by the $\chi^2_\nu < 2.0$. However, a randomly selected sample of residuals was examined by eye to ensure that they were indeed predominately noise dominated. The $\chi^2_\nu < 2.0$ criterion was therefore

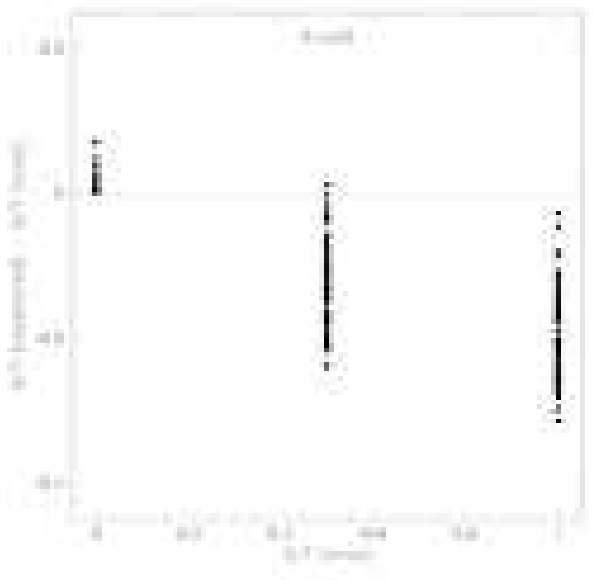


Figure A5. The difference between input and recovered values of S/T using GIM2D for a set of 250 model galaxies. The mean offset in the recovered values are $\Delta S/T = 0.02$ (for $S/T = 0.0$), $\Delta S/T = 0.13$ (for $S/T = 0.5$) and $\Delta S/T = 0.20$ (for $S/T = 1.0$). Model galaxies span a range of apparent magnitudes, sizes and orientations.

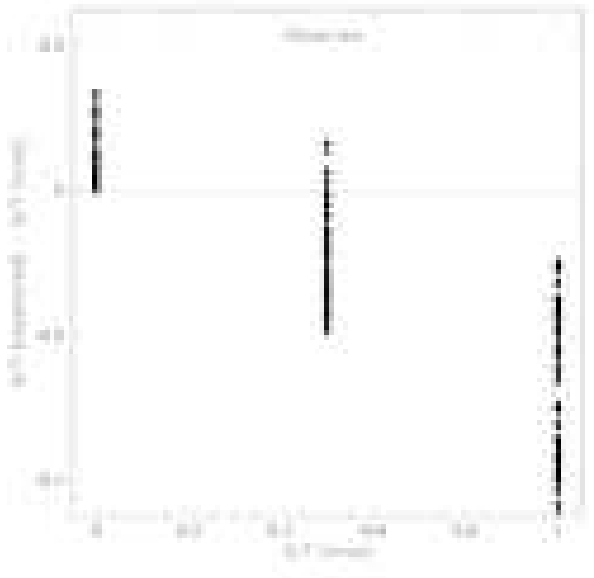


Figure A6. The difference between input and recovered values of S/T using GALACTICA for a set of 250 model galaxies. The mean offset in the recovered values are $\Delta S/T = 0.05$ (for $S/T = 0.0$), $\Delta S/T = 0.11$ (for $S/T = 0.5$) and $\Delta S/T = 0.24$ (for $S/T = 1.0$). Model galaxies span a range of apparent magnitudes, sizes and orientations. The median $\Delta S/T$ is well fit by the relation $\Delta S/T = 0.02 - 0.26S/T_{\text{true}}$.

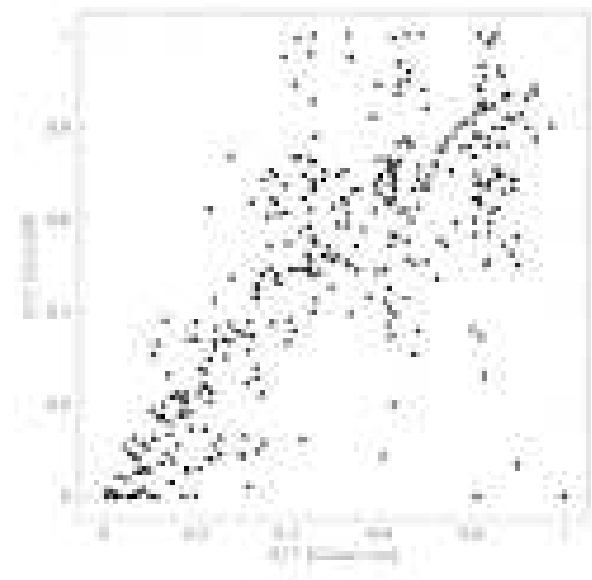


Figure A7. The correlation between the S/T ratios of a sample of 350 SDSS galaxies inferred using GIM2D and GALACTICA. The Spearman rank correlation coefficient of 0.74 indicates a significant correlation. Note that almost no pure disks (i.e. $S/T = 0.0$) are detected by GALACTICA but a few are detected by GIM2D. Most of these galaxies have spheroid characteristic radii of less than 2 pixels (as does the single GALACTICA detection at $S/T = 1.0$). GIM2D finds larger characteristic radii for these galaxies. The overall scatter is $\sigma_{\text{rms}} = 0.19$, but there is a marked increase in the scatter for larger S/T ratios.

adopted to define a ‘well fit’ dataset of 7493 galaxies. To test for any selection biases were introduced by the rejection of galaxies with $\chi^2_{\nu} > 2.0$, we compare the distributions of some basic properties of these galaxies and of the well-fit subset in Fig. B5. There are small but noticeable biases introduced in the distributions of apparent magnitudes and redshifts. These biases are taken into account when estimating galaxy luminosity functions (see §4.3) The figure also shows a deficit of objects with $S/T > 0.7$. This is most likely due to the bias in the GALACTICA code discussed in Appendix A. The significance of this bias and its influence on the final results is discussed in the main body of the paper.

Finally, in Fig. B6 we plot the distribution of R_{50} (the radius enclosing 50% of the Petrosian flux) for galaxies meeting the selection criteria of this work and that of Tasca & White (2006). Our galaxies are typically 40% smaller than those of Tasca & White (2006).

B3 S/T error estimates

Benson et al. (2002) developed a Monte Carlo approach to estimate the errors on the fitted parameters in GALACTICA. This method is very time consuming, requiring several CPU days for a typical galaxy. A full Monte Carlo analysis is therefore impractical for a large dataset such as the one in this paper. Instead, to obtain representative error estimates, we split the sample into bins of apparent magnitude of width 0.5, and selected from each of these bins 5 galaxies from each of three further bins in S/T ($0.0 < S/T < 0.3$, $0.3 < S/T <$

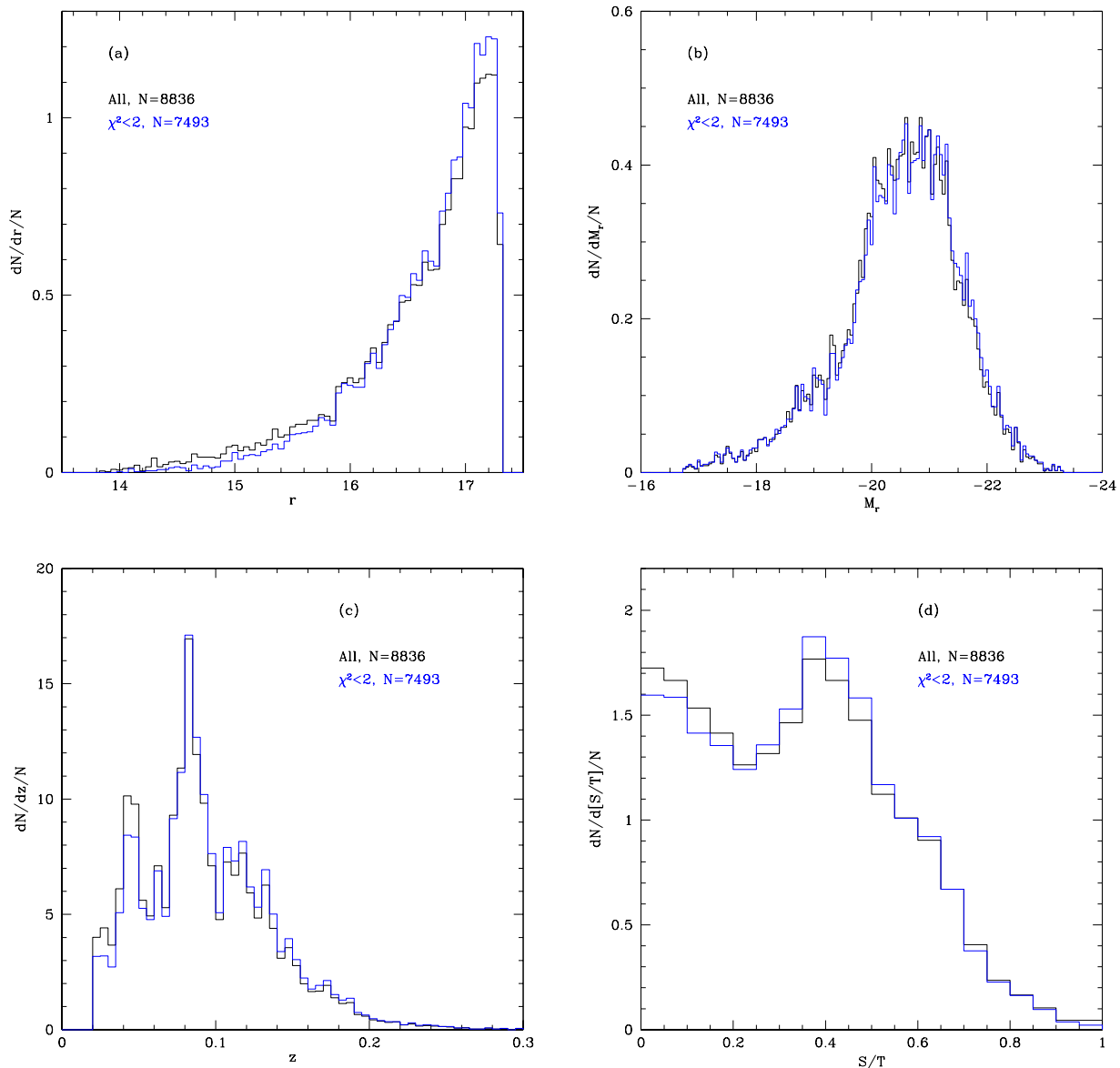


Figure B5. Distributions of (a) apparent magnitude, (b) absolute magnitude, (c) redshift and (d) recovered S/T ratios. Results for the total sample are shown by the black histograms and for the sample with $\chi^2 < 2.0$ by the blue histograms. The two distributions are similar, indicating that excluding poorly fit galaxies does not introduce any obvious biases in the sample.

0.6, $0.6 < S/T < 1.0$). The full Monte Carlo analysis was performed on the selected subsample and the medians of the derived errors taken to be representative for galaxies in each $[r_{\text{mag}}, S/T]$ bin.

APPENDIX C: SPHEROID-TO-DISK RATIOS AND GALAXY MORPHOLOGIES

C1 Morphological classification using colour

It has long been known that galaxy colour is a useful indicator of whether a galaxy is elliptical (old, red) or spiral (young, blue) (de Vaucouleurs 1961) since the dominant stellar populations are reflected in the galaxy colours. Invest-

igating the colour-magnitude and colour-colour diagrams, Strateva et al. (2001) have shown that the $(u-r)$ colour distribution of SDSS galaxies has two maxima which are separated by a well-defined minimum at $(u-r) = 2.2$ and that 98% of galaxies spectroscopically classified as ‘early’ types have $(u-r) > 2.2$ whilst 73% of spectroscopically classified ‘late’ types have $(u-r) < 2.2$. Strateva et al. (2001) have also shown that this separator also applies for a subsample of visually classified morphological types where 80% of galaxies visually classified as E, S0 or Sa have colours redder than $(u-r) = 2.2$ and 66% of galaxies visually classified as Sb, Sc and Irr have colours bluer than $(u-r) = 2.2$. The $(u-r)$ separator has already been used to study morpholog-

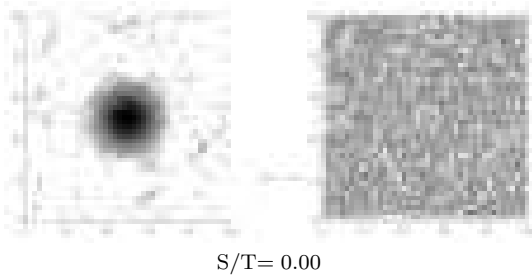


Figure B1. Fit to a pure exponential model galaxy after the original 101×101 model image was binned 2×2 . The top row shows the real (left) and model (right) images. The middle row shows the disk (left) and spheroidal (right) components. The bottom row shows the real (left) and residual (right) images. The recovered $S/T = 0$, corresponding to a pure exponential. The good fit is evident from both the $\chi^2_\nu \sim 1$ and the noise-dominated residual image.

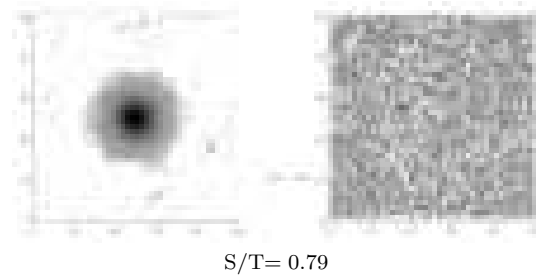


Figure B2. Fit to a pure $r^{1/4}$ model galaxy after the original 101×101 model image was binned 2×2 . The top row shows the real (left) and model (right) images. The middle row shows the disk (left) and spheroidal (right) components. The bottom row shows the real (left) and residual (right) images. The recovered $S/T = 0.8$, showing once more that the GALACTICA code returns a biased estimate of S/T . The good fit is inferred from both $\chi^2_\nu \sim 1$ and the noise-dominated residual image.

ical properties of galaxies in the SDSS sample as a function of environment (Goto et al. 2002; Balogh et al. 2004).

Our derived S/T ratios are plotted against $u-r$ colour in Fig. C1. The B/T distributions of red galaxies and blue galaxies are significantly displaced relative to each other: most galaxies classified by colour as early types ($u-r > 2.2$) have $S/T > 0.4$ whereas most galaxies classified by colour as late types ($u-r < 2.2$) have $S/T < 0.2$. However, the red galaxies in particular span a large range in S/T ratio. This suggests that blue star-forming galaxies are predominantly disk-dominated but that disk-dominated galaxies include both star-forming (blue) and passive (red) galaxies⁶

C2 Morphological classification using concentration index

Galaxies can also be classified according to how ‘peaky’ their light distribution is by using the concentration index (Abraham et al. 1994). The surface brightness distribution of

ellipticals and S0s is considerably more centrally concentrated than that of spirals and irregulars. Shimasaku et al. (2001) defined the (inverse) concentration index for SDSS galaxies as the ratio of the half- to the 90% light radii and define an optimum division between late and early types to be at $C = 0.33$ (with 15 – 20% contamination from opposite types). This separator has also been used to investigate the morphological properties of SDSS galaxies (Goto et al. 2002; Nakamura et al. 2003).

Fig. C2 shows that there is a good correlation between the S/T ratios and the (inverse) concentration index, C , for galaxies with small $S/T \lesssim 0.3$. Although spheroid-dominated galaxies tend to be more centrally concentrated than disk-dominated galaxies, there is little correlation of concentration with S/T for $S/T \gtrsim 0.3$. There is, however, considerable scatter in C for a given S/T .

C3 Morphological classification: S/T vs eye-morphology

Shimasaku et al. (2001) used a sample of 456 bright SDSS galaxies ($g' < 16.0$) visually classified into seven morphological types (Hubble types E, S0, Sa, Sb, Sc, Sdm and Im) to in-

⁶ The red disk population may also include galaxies with heavily obscured star formation.

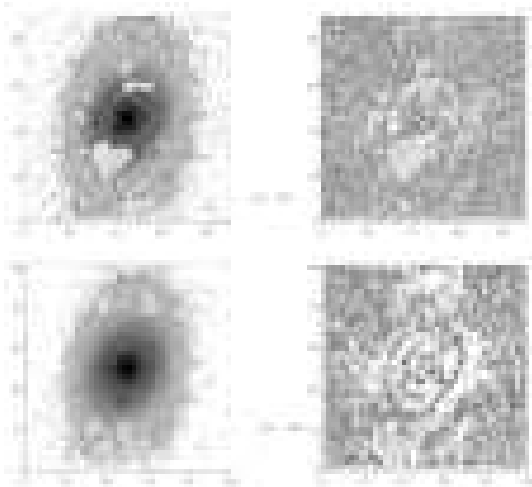


Figure B3. Fits to a galaxy that exhibits internal structure. The top images show the unbinned galaxy postage-stamp (left) and the corresponding residual image (right). The bottom images show the galaxy and the residual after the galaxy is binned 2×2 . In both cases the χ^2_ν is poor ($\chi^2_\nu > 2.0$) and the residuals are not noise-dominated. This supports the conclusion that galaxies with significant structure give poor fits irrespective of whether they are binned or not.

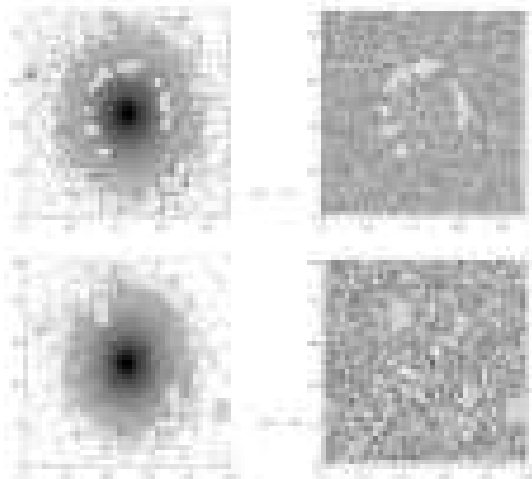


Figure B4. Fits to a galaxy that does not exhibit internal structure. The top images show the unbinned galaxy postage-stamp (left) and the corresponding residual image (right). The bottom images show the galaxy and the residual after the galaxy is binned 2×2 . In both cases, the χ^2_ν is good ($\chi^2_\nu < 2.0$) and the residuals are noise-dominated. This supports the conclusion that galaxies without significant structure result in acceptable fits irrespective of whether they are binned or not.

investigate correlations between galaxy colours, effective sizes and concentrations. The (inverse) concentration index was found to correlate well with the visual estimates of morphology. Shimasaku et al. (2001) have kindly provided us with their visual morphologies in order to compare them with the GALACTICA S/T ratios. There are 166 galaxies in common in the two samples which have $\chi^2_\nu < 2.0$. Fig. C3 shows that there is a fair correlation between the (inverse) concentration

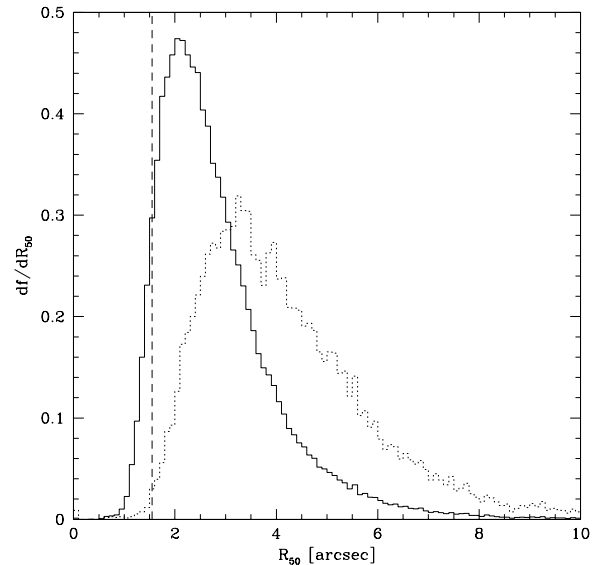


Figure B6. The distribution of R_{50} (the radius enclosing 50% of the Petrosian flux) for galaxies in the SDSS which match our selection criteria (solid histogram). Results are also shown for the sample used by Tasca & White (2006) (dotted histogram). For comparison, we indicate the maximum allowable seeing for our sample by the vertical dashed line.

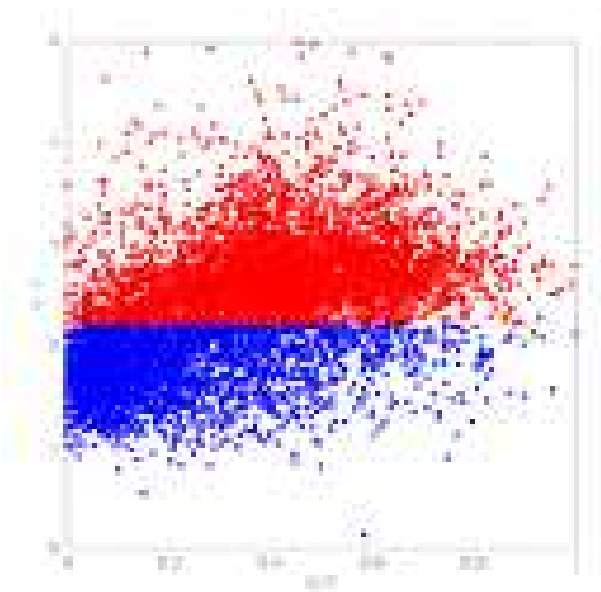


Figure C1. GALACTICA S/T ratio vs. $(u-r)$ colour for the sample of 7493 SDSS galaxies studied here. Most galaxies colour-classified as late types are predominately disk-dominated systems while most galaxies colour-classified as early type have $S/T > 0.4$.

index and the visual morphology for these 166 galaxies, confirming the conclusions of Shimasaku et al. (2001). Plotted in Fig. C4 is the correlation between our derived S/T ratios and the visual morphology for these galaxies. Although the scatter is large, there is a clear trend for the earlier types to have larger S/T ratios.

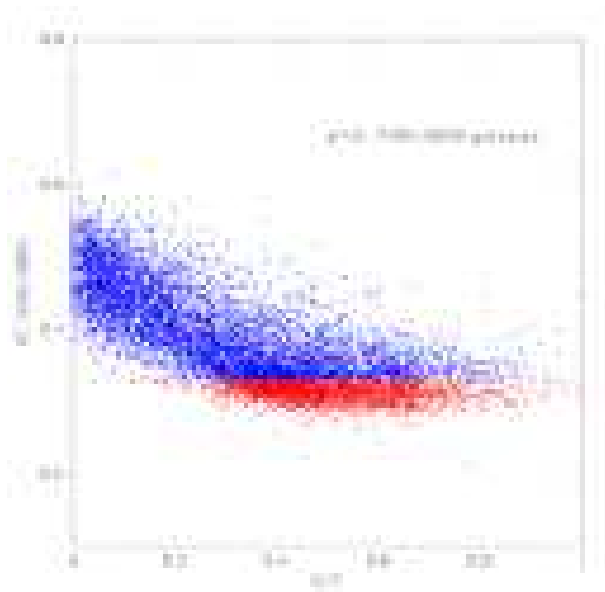


Figure C2. GALACTICA S/T ratio vs. (inverse) concentration index, $C = R_{50}/R_{90}$, for our sample of 7493 SDSS galaxies. More centrally concentrated galaxies ($C < 0.33$) predominately have higher S/T ratios.

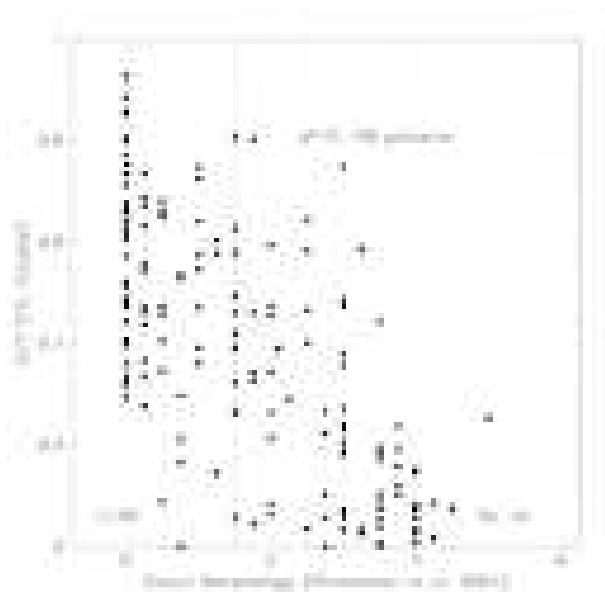


Figure C4. GALACTICA S/T ratio vs. the visual morphology determined by Shimasaku et al. (2001) for the 166 galaxies in common in the two sample. There is a general trend for the S/T ratio to increase along the S-S0-E morphological sequence but the scatter is large.

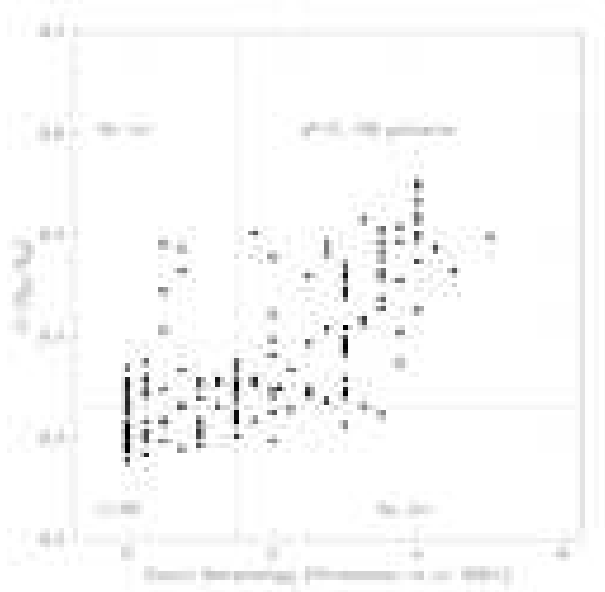


Figure C3. Concentration index vs. eye morphology for 166 galaxies in common between our sample and that of Shimasaku et al. (2001).